Dear Editor, Journal of Nonlinear Processes in Geophysics

We would like to thank you for the letter dated 25/09/2020, and the opportunity to resubmit a revised copy of this manuscript. We would also like to take this opportunity to express our thanks to the reviewers for the positive feedback and helpful comments for correction or modification.

We believe it has resulted in an improved revised manuscript. The manuscript has been revised to address the reviewer comments, which are appended alongside our responses to this letter.

We very much hope the revised manuscript is accepted for publication in the Journal of Nonlinear Processes in Geophysics.

Sincerely yours,
Cristian Lussana on behalf of the authors

In the interactive discussion, our answers to the reviewers comments include point-by-point responses to the reviews. A list of the relevant changes follows:

- Better description of the data transformation. We have revised Secs. 2.1 - 2.2 and 3.3. Adjusted the algorithm and the tables with the mathematical notations. We have Introduced the scalar variables α_D and β_D defining the gamma distribution used in the data transformation. We have Introduced the vectors α^A and β^A defining the gamma distributions of hourly precipitation at grid points. The coefficient previously denoted with α is now ν. Fig 8 is new and it serves two purposes: It shows an example of data transformation and it supports our choice of using a Gamma cumulative distribution function in the transformation.

- The "stabilization factor" has been renamed as "inflation factor" and it has been introduced and described in a better way than before.

- Reviewer 2 suggested to refer to EnKF instead of EnOI, because EnOI makes use of a time-lagged ensemble. We have modified the statement when we are referring to EnOI to point out the differences. However, we still make a connection between EnSI-GAP and EnOI, since the EnSI-GAP equations are more similar to EnOI than EnKF.

- We have tried to implement the suggestion of Reviewer2 on renaming the "scale matrix" as the "static covariance matrix". However, the term "static covariance matrix" is rather general and it may generate confusion. For instance, the observation error covariance matrix is also a static covariance matrix. In addition, the scale matrix may change every hour and in this sense it is not static. To avoid confusion, we should have replaced the "scale matrix" with "static background error covariance matrix", which is too long. We keep the term "scale matrix" and we have added a disambiguation on the fact that we are not referring to "spatial scales".

- Working assumptions introduced in Sec. 2.2.2. We have almost entirely rewritten

Sec. 2.2.2 and adapted Sec. 2.2.3. The working assumptions are first formulated as general principles, then at the end of the section they are rewritten in more precise mathematical terms with links to the corresponding equations. We have also linked the different parts in the text where they are used.

- Section 3. Results. This section has been almost completely rewritten. It has been also better organized in subsections. The figures referring to this section have been modified and new figures have been added. Two figures have been removed (Figs. 13 and 14).

- We discuss other ways to determine the background error covariance matrices, in addition to those used in the manuscript, in Sec 3.1.6. The reader could also find the other methods in the literature we cite.

- Section 3.1 has been completely rewritten, new results have been added, Figures have been re-plotted. The same simulation as before has been considered, moreover we have extended the considerations to 100 simulations similar to the one presented. This way, our conclusions are more general, since they are not related to a single case. The interpretation of results is more quantitative and less qualitative, thanks to the introduction of two scores MSESS and CRPS. The session is now better organized, because of the subdivision into subsections. Figs. 2-6 are either new or re-done. Table 3 summarizes the statistics of results over 100 simulations.

- Figures 8 and 10 (ex-figures 6 and 8) have been modified to emphasize the region where the observations are not available. In Fig. 8 we have also added the Sogn og Fjordane box. Fig 10 has isolines.

Ensemble-based statistical interpolation with Gaussian anamorphosis for the spatial analysis of precipitation

Cristian Lussana[1], Thomas N. Nipen[1], Ivar A. Seierstad[1], and Christoffer A. Elo[1]

[1]Norwegian Meteorological Institute, Oslo, Norway

Correspondence: Cristian Lussana (cristianl@met.no)

Abstract. Hourly precipitation over a region is often simultaneously simulated by numerical models and observed by multiple data sources. An accurate precipitation representation based on all available information is a valuable result for numerous applications and a critical aspect of climate monitoring. Inverse problem theory offers an ideal framework for the combination of observations with a numerical model background. In particular, we have considered a modified ensemble optimal interpo-

5 lation scheme, that takes into account deficiencies of the background. An additional source of uncertainty for the ensemble background has been included. The deviations between background and observations are used to adjust for deficiencies of the ensemble. A data transformation based on Gaussian anamorphosis has been used to optimally exploit the potential of the spatial analysis, given that precipitation is approximated with a gamma distribution and the spatial analysis requires normally distributed variables. For each point, the spatial analysis returns the shape and rate parameters of its gamma distribution. The

10 Ensemble-based Statistical Interpolation scheme with Gaussian AnamorPhosis (EnSI-GAP) is implemented in a way that the covariance matrices are locally stationary and the background error covariance matrix undergoes a localization process. Concepts and methods that are usually found in data assimilation are here applied to spatial analysis, where they have been adapted in an original way to represent precipitation at finer spatial scales than those resolved by the background, at least where the observational network is dense enough. The EnSI-GAP setup requires the specification of a restricted number of parameters

15 and specifically the explicit values of the error variances are not needed, since they are inferred from the available data. The examples of applications presented over Norway provide a better understanding of the characteristics of EnSI-GAP. The data sources considered are those typically used at national meteorological services, such as local area models, weather radars and in-situ observations. For this last data source, measurements from both traditional and opportunistic sensors have been considered.

1 Introduction

Precipitation amounts are measured or estimated simultaneously by multiple observing systems, such as networks of automated weather stations and remote sensing instruments. At the same time, sophisticated numerical models simulating the evolution of the atmospheric state provide a realistic precipitation representation over regular grids with spacing of a few kilometers. An unprecedented amount of rainfall data is nowadays available at very short sampling rates of one hour or less. Nevertheless, it is common experience within national meteorological services that the exact amount of precipitation, to some extent, eludes our knowledge. There may be numerous reasons for this uncertainty. For example, a thunderstorm triggering a landslide may have occurred in a region of complex topography where in-situ observations are available but not exactly on the landslide spot, weather radars cover the region in a patchy way because of obstacles blocking the beam, and numerical weather prediction forecasts are likely misplacing precipitation maxima. Another typical situation is when an intense and localized summer thunderstorm hits a city. In this case, several observation systems are measuring the event and more than one numerical model may provide precipitation totals. From this plurality of data, a detailed reconstruction of the event is possible, provided that the data agrees both in terms of the event intensity and on its spatial features. This is not always the case and sometimes meteorologists and hydrologists are left with a number of slightly different but plausible scenarios.

The objective of our study is the precipitation reconstruction through the combination of numerical model output with observations from multiple data sources. The aim is that the combined fields will provide a more skillful ~~prediction~~ representation than any of the original data sources. As remarked above, any improvement in the accuracy and precision of precipitation can be of great help for monitoring the weather, but not only that. Snow- and hydrological- modeling will benefit from improvements in the quality of precipitation, which is one of the atmospheric forcing variables (**??**). Climate applications that make use of reanalysis (e.g. **??**) or observational gridded datasets (e.g. **?**), as for instance the evaluation of regional climate model (**?**) or the calculation of climate indices (**?**), may also benefit from datasets combining model output and observations, as shown by **?**. Besides, the intensity-duration-frequency curve (IDF curve) derived from precipitation datasets are widely used in civil engineering for determining design values and the quality of the reconstruction of extremes has a strong influence on IDF curves (**?**).

The data source considered in our study are precipitation ensemble forecasts, observations from in-situ measurement stations and estimates derived from weather radars. Numerical model fields are available everywhere and the quality of their output is constantly increasing over the years. The weather-dependent uncertainty is often delivered in the form of an ensemble. At present ~~for data-sparse regions, such as in the mountains, the quality~~, assessments using hydrological models have shown that input from numerical models "may be comparable or preferable compared to gauge observations to drive a hydrologic and/or snow model in complex terrain" as stated by (**?**) based on their review of recent research. One of the key messages by **?** is that numerical models represent precipitation fields at ungauged sites in a realistic and convincing way, as it is demonstrated by the accuracy of their total annual rain and snowfall estimates, notwithstanding that daily or sub-daily aggregated precipitation fields may misrepresents individual precipitation events, such as storms. In the work by **?**, it has been demonstrated that the combination of numerical model output ~~in modeling rain and snow is comparable or even better than those of observational~~

networks (?)and in-situ observations do improve the representation of monthly precipitation climatologies over Norway, if compared to similar products based on in-situ observations only. ? have successfully used monthly precipitation climatologies to improve the performances of statistical interpolation methods in complex terrain over Norway. However, because model fields represent areal averages, the characteristics of simulated precipitation depend significantly on the model resolution, as remarked for global and regional reanalyses over the Alps by ?. In particular, ? demonstrates that increasing resolution via downscaling improves precipitation representation, though they also point out that assimilating observations at high resolution in numerical models is important for reconstructing high-threshold/small-scale events. The sources of model errors and their treatments in data assimilation (DA) schemes have been studied extensively. For instance, in the introduction of the paper by ?, a list of model errors is reported together with several references to other studies addressing them. Regarding precipitation forecasts, model errors often encountered in applications are (?): systematic under- or overestimation of amounts; spatial errors in the placement of events; underestimation of uncertainty. With reference to spatial analysis, we consider observed precipitation data to be more accurate than model estimates. In fact, model outputs are evaluated in their ability to reconstruct observed values. The most important disadvantage of observational networks is that often they do not cover the region under consideration, moreover observations may be irregularly distributed in space and present missing data over time. Each observational data source has its own characteristics that have been extensively studied in literature and that we will address here only superficially, since our objective is the combination of information. For example, rain gauges are possibly the most accurate precipitation measurement available at present (?), apart from when the observations are affected by gross measurement errors, as they have been defined by ?. There are multiple sources of uncertainty for gauge measurements (?), such as catching and counting (?). The undercatch of solid precipitation due to wind (?) is a significant problem in cold climates. Radar-derived estimates are affected by several issues, such as blocking and non-uniform attenuation of the radar beam due to obstacles along the path, especially in complex terrain. A statement in the Introduction of the book by ? is illuminating in this sense "To put a weather radar in a mountainous region is like pitching a tent in a snowstorm: the practical use is obvious and large — but so are the problems". In addition, weather radars do not directly measure precipitation, instead they measure reflectivity, which is then transformed into precipitation rate. The transformation itself contributes to increasing the uncertainty of the final estimates. Another important aspect of observational data that will be treated only marginally here is data quality control, in this work we will consider only quality controlled observations. To sum up, in-situ data are the more accurate observations of precipitation we will consider. Then, radar estimates, which are calibrated using gauges as references, are less accurate than in-situ data. They are spatially correlated with the actual precipitation and they are affected by less uncertainty than the simulations carried out by numerical models. Numerical model output is the basic information available everywhere and the one we consider more uncertain.

Inverse problem theory (?) provides the ideal framework for the combination of observations with a numerical model background. The marginal distribution of the precipitation analysis is assumed to be a gamma distribution and we aim at estimating its shape and rate parameters for each grid point. The gamma distribution is appropriate for representing precipitation data, as reported e.g. by ?. The formulation of the statistical interpolation method presented is similar to the ensemble Optimal Interpolation (?)analysis step of the ensemble Kalman filter ? or the ensemble optimal interpolation (EnOI ?) with

the important difference that EnOI uses a time-lagged ensemble, while the ensemble considered in our method is made of members of a single NWP model run. The hourly precipitation over the grid is regarded as the realization of ~~trans-gaussian~~ a transformed Gaussian random field (**?**). The Gaussian anamorphosis (**?**) transforms data such that precipitation better complies with the assumptions of normality that are required by the analysis procedure. The non-stationary covariance matrices are approximated with locally stationary matrices, as in the paper by **?**. In addition, the background error covariance matrix includes a static (i.e. not flow-dependent) scale matrix that accounts for deficiencies in the background ensemble as in hybrid ensemble optimal interpolation (**?**). The term scale matrix has been used by **?**. ~~The~~ In the following, the ensemble-based statistical interpolation with Gaussian anamorphosis for the spatial analysis of precipitation is referred to ~~in the following with the acronym of~~ as EnSI-GAP. From the point of view of geostatistics, EnSI-GAP can be thought of as performing a Kriging (**?**) of the Gaussian transformed ensemble mean, then retrieving the probability distribution of precipitation at every location using a predefined Gamma distribution.

The innovative part of the presented approach to statistical interpolation is in the application to spatial analysis of concepts that are usually encountered in DA. The formulation of the problem is adapted to our aim, which is improving precipitation representation instead of providing initial conditions for a physical model, as it is for DA. In the literature, there are a number of articles describing similar approaches applied to precipitation analysis, such as **???**. However, our statistical interpolation is the first one, ~~that we know of~~to our knowledge, where the background error covariance matrix is derived from numerical model ensemble and where Gaussian anamorphosis is applied directly to precipitation data. An additional innovative part of the method is that EnSI-GAP does not require the explicit specification of error variances for the background or observations, as most of the other methods (**?**). In fact, those error variances are often difficult to estimate in a way that is general enough to cover a wide range of cases. Our approach is to specify the reliability of the background with respect to observations, in such a way that error variances can vary both in time and space. An additional innovative part of our research is that we consider opportunistic sensing networks of the type described by **?** within the examples of applications proposed. Citizen weather stations are rapidly increasing in prevalence and are becoming an emerging source of weather information, as described by **?**. Thanks to those networks, for some regions we can rely on an extremely dense spatial distribution of in-situ observations.

The remaining of the paper is organized as follows. Sec. 2 describes the EnSI-GAP method in a general way, without references to specific data sources. Sec. **??** presents the results of EnSI-GAP applied to three different problems: an idealized ~~situation~~experiment, then two examples where the method is applied to real data~~, such as those mentioned above. The results are discussed in Sec. ??~~.

2 Methods: EnSI-GAP, Ensemble-based statistical interpolation with Gaussian anamorphosis for precipitation

We assume that the marginal probability density function (PDF) for the hourly precipitation at a point in time follows a gamma distribution (**?**). This marginal PDF is characterized through the estimation of the gamma shape and rate for each point and hour.

Precipitation fields are regarded as realizations of locally-stationary, ~~trans-Gaussian~~ transformed Gaussian random fields, where each hour is considered independently from the others. ~~Trans-Gaussian~~ The time sequence of EnSI-GAP simulated precipitation fields do show temporal continuity because this is present in both observations and background fields. Transformed Gaussian random fields are used for the production of precipitation observational gridded datasets by **?**. A random field is said to be stationary if the covariance between a pair of points depends only on how far apart they are located from each other. Precipitation totals are nonstationary random fields because ~~the covariance between a pair of points in space depends not only on the distance between them but it varies also when considered in different directions~~of the nonstationarity of weather phenomena or simply the influence of topography. In our method, precipitation is locally modeled as a stationary random field. The covariance parameter estimation and spatial analysis are carried out in a moving-window fashion around each grid point. A similar approach is described by **?** and the elaboration over the grid can be carried out in parallel for several grid points simultaneously.

~~A particular~~ An implementation of EnSI-GAP is reported in Algorithm 4. The mathematical notation and the symbols used are described in two tables: Tab. 1 for global variables and Tab. 2 for local variables, which are those variables that vary from point to point. As in the paper by **?**, upper accents have been used to denote local variables. If $\mathbf{X}$ is a matrix, $\mathbf{X}_i$ is its ith column (column vector) and $\mathbf{X}_{i,:}$ is its ith row (row vector). The Bayesian statistical method used in our spatial analysis is optimal for Gaussian random fields. Then, a data transformation is applied as a pre-processing step before the spatial analysis. The introduction of a data transformation compels us to inverse transform the predictions of the spatial analysis back into the original space of precipitation values.

The data transformation chosen is a Gaussian anamorphosis (**?**), that transforms a random variable following a gamma distribution into a standard Gaussian. In the implementation presented, constant values of the gamma parameters shape and rate are used in the data transformation over the whole domain. The same values are used for the inverse transformation as well. The constant (in space) values are re-estimated every hour. It is worth remarking that the gamma parameters used in the data transformations must not be confused with those defining the gamma distribution of the hourly precipitation at each grid point and that are the objective of our spatial analysis. The analysis procedure returns a different Gaussian PDF for each grid point, which is transformed into a gamma distribution by means of the constant shape and rate estimated for the data transformation. However, since the inverse transformation at each grid point is applied to a Gaussian PDF that differs from those of the surroundings points, then the gamma distribution of hourly precipitation will also vary from one grid point to the other. The gamma shape and rate parameters used in the data transformation are denoted as the scalar values α_D and β_D, respectively, while the spatially dependent gamma analysis parameters are denoted with the m column vectors $\boldsymbol{\alpha}^{\mathrm{a}}$ and $\boldsymbol{\beta}^{\mathrm{a}}$.

Algorithm 4 can be divided into three parts, that are described in the next sections: the data transformation in Sec. 2.1, the Bayesian spatial analysis in Sec. 2.2 and the inverse transformation in Sec. **??**.

2.1 Data transformation via Gaussian anamorphosis

The ~~data transformation chosen is a Gaussian anamorphosis (?), that transforms a random variable following~~ Gaussian anamorphosis maps a gamma distribution into a standard Gaussian. **?** introduced the concept of Gaussian anamorphosis from geostatistics

to data assimilation. A general reference on Gaussian anamorphosis in geostatistics is the book by **?**, Chapter 6. This pre-processing strategy has been used in several studies in the past, e.g. **??**. A visual representation of the transformation process can be found in Fig. 1 of the paper by **?** and in this article in Sec. **??**.

The hourly precipitation background and observations, $\tilde{\mathbf{X}}^{\mathrm{f}}$ and $\tilde{\mathbf{y}}^{\mathrm{o}}$ respectively, are transformed into those used in the spatial analysis by means of the Gaussian anamorphosis $g()$:

$$\mathbf{X}^{\mathrm{f}} \;=\; g(\tilde{\mathbf{X}}^{\mathrm{f}}) \tag{1}$$

$$\mathbf{y}^{\mathrm{o}} \;=\; g(\tilde{\mathbf{y}}^{\mathrm{o}}) \tag{2}$$

As indicated in Tab. 1, the Gaussian variables are $\mathbf{X}^{\mathrm{f}}$ and $\mathbf{y}^{\mathrm{o}}$, while the variables with the original hourly precipitation values, $\tilde{\mathbf{X}}^{\mathrm{f}}$ and $\tilde{\mathbf{y}}^{\mathrm{o}}$, follow a gamma distribution. The gamma shape and rate α_D and β_D, respectively, of this gamma distribution are derived from the background precipitation values by a fitting procedure based on maximum likelihood. ~~The~~

In this paragraph, the procedure used in Sec. **??** is described. For an arbitrary hour, two different solutions are adopted, depending on the weather conditions. We are in the presence of dry weather conditions when at least one of the ensemble members reports precipitation in less than 10% of the grid points, otherwise we have wet weather. In case of wet conditions, ensemble members are considered separately and for each of them we derive a single value of shape and a single value of rate, both are kept constants over the whole domain. The values of shape and rate are the maximum likelihood estimators ~~are~~ calculated iteratively by means of a Newton-Raphson method as described by **?**, Sec. 4.6.2. ~~In particular, the gamma distribution parameters are fitted to each ensemble member field of precipitation separately. Then, the averaged shape~~ Then, α_D and ~~rate are used in $g()$ for Eqs.~~ β_D are the averages of all the values of shape (one value for each ensemble member) and rate (one value for each ensemble member). In case of dry weather, α_D and β_D are set to "typical" values obtained as the averages of all the available cases.

In Gaussian anamorphosis, zero precipitation values must be treated as special cases, as explained by **?**. The solution we adopted is to add a very small amount to zero precipitation values, ~~e.g. 0.0001 mm~~ $\xi = 0.0001$mm, then to apply the transformation $g()$ to all values. The same small amount is then subtracted after the inverse transformation. This is a simple but effective solution for spatial analysis, as shown in the example of Sec. **??**. In principle, the statistical interpolation is sensitive to the small amount ξ chosen, such that using 0.01 mm instead of 0.0001 mm will return slightly different analysis values in the transition between precipitation and no-precipitation. In practice, we have tested it and we found negligible differences when values smaller than e.g. 0.05 mm (half of the precision of a standard rain gauge measurement) have been used.

The transformation function $g(x)$, applied to the generic scalar value x, used in Eqs. (1)-(2) is:

$$g(x) = Q_{\mathrm{Norm}}\left(\mathrm{Gamma}(x + \xi; \alpha_D, \beta_D)\right) \tag{3}$$

where $\mathrm{Gamma}(x + \xi; \alpha_D, \beta_D)$ is the gamma cumulative distribution function when the shape is equal to α_D and the rate is equal to β_D. Q_{Norm} is the quantile function (or inverse cumulative distribution function) for the standard Gaussian distribution. An example of application of the procedure described above is given in Sec. **??**.

For the presented implementation of EnSI-GAP, the Gaussian anamorphosis is based on the constant parameters α_D and β_D over the whole domain. This assumption might be too restrictive for very large domains, such as for all Europe for instance.

In this case, different solutions may be explored such as slowly varying the gamma parameters in space, or time, based on the climatology.

2.2 Spatial analysis

The spatial analysis inside Algorithm 4 has been divided into three parts. In Sec. 2.2.1, global variables have been defined. Then, as stated in the introduction of Sec. 2, the analysis procedure is performed on a gridpoint-by-gridpoint basis. In Sections 2.2.2-**??**, the procedure applied at the generic ith gridpoint is described. In Sec. 2.2.2, the specification of the local error covariance matrices is described. In Sec. **??**, the standard analysis procedure is presented together with the treatment of a special case.

2.2.1 Definitions

In Bayesian statistics, according to **?**, a state is "a description of the world, which is the object which we are concerned, leaving no relevant aspect undescribed" and "the true state is the state that does in fact obtain". The mathematical notation used is reported in Tab. 1- 2 and it is similar to that suggested by **?**. The object of our study is the hourly precipitation field $x()$, that is the hourly total precipitation amount over a continuous surface covering a spatial domain in terrain-following coordinates $\mathbf{r}$. Our state is the discretization over a regular grid of this continuous field. The true state (our "truth", $\mathbf{x}^{\mathrm{t}}$) at the ith grid point is the areal average:

$$\mathbf{x}_i^{\mathrm{t}} = \int_{V_i} x\left(\mathbf{r}\right) \mathrm{d}\mathbf{r} \tag{4}$$

where V_i is a region surrounding the ith grid point. The size of V_i determines the effective resolution of $\mathbf{x}^{\mathrm{t}}$ at the ith grid point. Our aim is to represent the truth with the smallest possible V_i. The effective resolution of the truth will inevitably vary across the domain. In observation-void regions, the effective resolution will be the same as that of the numerical model used as the background, then approximately $o(10-100\,km^2)$ for high-resolution local area models (**?**). In observation-dense regions, the effective resolution should be comparable to the average distance between observation locations, with the model resolution as the upper bound.

The analysis is the best estimate of the truth, in the sense that it is the linear, unbiased estimator with the minimum error variance. The analysis is defined as $\mathbf{x}^{\mathrm{a}} = \mathbf{x}^{\mathrm{t}} + \boldsymbol{\eta}^{\mathrm{a}}$, where the column vector of the analysis error at grid points is a random variable following a multivariate normal distribution $\boldsymbol{\eta}^{\mathrm{a}} \sim \mathcal{N}\left(\mathbf{0}, \mathbf{P}^{\mathrm{a}}\right)$. The marginal distribution of the analysis at the ith grid point is a normal random variable and our statistical interpolation scheme returns its mean value $\mathbf{x}_i^{\mathrm{a}}$ and its standard deviation $\sigma_i^{\mathrm{a}} = \sqrt{\mathbf{P}_{ii}^{\mathrm{a}}}$.

As for linear filtering theory (**?**), the analysis is obtained as a linear combination of the background (a priori information) and the observations. The background is written as $\mathbf{x}^{\mathrm{b}} = \mathbf{x}^{\mathrm{t}} + \boldsymbol{\eta}^{\mathrm{b}}$, where the background error is a random variable $\boldsymbol{\eta}^{\mathrm{b}} \sim N\left(\mathbf{0}, \mathbf{P}^{\mathrm{b}}\right)$. The background PDF is determined mostly, but not exclusively, by the forecast ensemble, as described in Sec. 2.2.1. The forecast ensemble mean is $\mathbf{x}^{\mathrm{f}} = k^{-1}\mathbf{X}^{\mathrm{f}}\mathbf{1}$, where $\mathbf{1}$ is the m-vector with all elements equal to 1. The background expected value is set to the forecast ensemble mean, $\mathbf{x}^{\mathrm{b}} = \mathbf{x}^{\mathrm{f}}$. The forecast perturbations are $\mathbf{A}^{\mathrm{f}}$, where the ith perturbation is $\mathbf{A}_i^{\mathrm{f}} = \mathbf{X}_i^{\mathrm{f}} - \mathbf{x}^{\mathrm{f}}$.

The covariance matrix:

$$\mathbf{P}^{\mathrm{f}} = (k-1)^{-1}\mathbf{A}^{\mathrm{f}}\mathbf{A}^{\mathrm{fT}} \tag{5}$$

plays a role in the determination of $\mathbf{P}^{\mathrm{b}}$, as defined in Sec. 2.2.2.

The p observations are written as $\mathbf{y}^{\mathrm{o}} = \mathbf{H}\mathbf{x}^{\mathrm{t}} + \boldsymbol{\varepsilon}^{\mathrm{o}}$, where the observation error is $\boldsymbol{\varepsilon}^{\mathrm{o}} \sim N(\mathbf{0}, \mathbf{R})$ and $\mathbf{H}$ is the observation operator, that we consider as a linear function mapping $\mathbb{R}^m$ onto $\mathbb{R}^p$.

2.2.2 Specification of the observation and background error covariance matrices

Our definitions of the error covariance matrices follow from a few ~~working assumptions, WA*n* indicates the *n*th working assumption and the abbreviations will be used in the text. WA1~~general principles that we have formulated. P1 (i.e. general principle 1), background and observation uncertainties are weather- and location- dependent. ~~WA2~~P2, the background is more uncertain where either the forecast is more uncertain or observations and forecasts disagree the most. ~~WA3~~P3, observations are a more accurate estimate of the true state than the background. We want to specify how much more we trust the observations than the background in a simple way, such as e.g. "we trust the observations twice as much as the background". ~~WA4~~P4, the local observation density must be used optimally to ensure a higher effective resolution, as it has been defined in Sec. 2.2.1, where more observations are available. ~~WA5~~P5, the spatial analysis at a particular hour does not require the explicit knowledge of observations and forecasts at any other hour. However, constants in the covariance matrices can be set depending on the history of deviations between observations and forecasts. ~~WA5~~ P5 makes the procedure more robust and easier to implement in real-time operational applications.

P1 and P4 led to our choice of implementing Algorithm 4 by means of loop over grid points.

A distinctive feature of our spatial analysis method is that the background error covariance matrix $\overset{i}{\mathbf{P}}{}^{\mathrm{b}}$ is specified as the sum of two parts: a dynamical component and a static component. This choice is consistent with P1 and P2. The dynamical part introduces nonstationarity, while the static part describes covariance stationary random variables. This choice follows from ~~WA1~~ P1 and it has been inspired by hybrid data assimilation methods (**?**). The dynamical component of the background error covariance matrix is obtained from the forecast ensemble. Because the ensemble has a limited size, and often the number of members is quite small (order of ~~tenths of member~~tens of members), a straightforward calculation of the background covariance matrix will include spurious correlations between distant points. Localization is a technique applied in DA to fix this issue (**?**). The static component has also been introduced to remedy the shortcomings of using numerical weather prediction as the background. There are deviations between observations and forecasts that cannot be explained by the forecast ensemble. A typical example is when all the ensemble members predict no precipitation but rainfall is observed. In those cases, we trust observations, as stated through ~~WA3~~P3. Then, the static component adds noise to the model-derived background error, as in the paper by **?**. In **?**, the static component is referred to as a scale matrix, since it is used to scale the noise component of the model error, and we adopt the same term here. In scale matrix, the term "scale" is not associated with the concept of "spatial scales", instead it refers to a scaling (amplification or reduction) of the uncertainty. We will also refer to this matrix, and its related quantities, with the letter u to emphasize that this component of the background error is "unexplained" by the forecast.

255    $\overset{i}{\mathbf{P}}{}^{\mathrm{b}}$ is written as:

$$\overset{i}{\mathbf{P}}{}^{\mathrm{b}} = \overset{i}{\boldsymbol{\Gamma}} \circ \mathbf{P}^{\mathrm{f}} + \overset{i}{\sigma}_u^2 \overset{i}{\boldsymbol{\Gamma}}{}^{\mathrm{u}} \tag{6}$$

The first component on the right-hand side of Eq. (5) is the dynamical part. $\mathbf{P}^{\mathrm{f}}$ is the forecast uncertainty of Eq. (4), $\overset{i}{\boldsymbol{\Gamma}}$ is the localization matrix and $\circ$ is the Schur product symbol. The localization technique we apply is a combination of local analysis and covariance localization, as they have been defined by **?**. In the local analysis, only the closest observations are used and we

260   have implemented it by considering only observations within a predefined spatial window surrounding each grid point, up to a pre-set maximum number of p_{mx}. The covariance localization is implemented through the element-wise multiplication of $\mathbf{P}^{\mathrm{f}}$ by $\overset{i}{\boldsymbol{\Gamma}}$, which has the form of a correlation matrix that depends on distances and that is used to suppress long-range correlations. The second component on the right-hand side of Eq. (5) is the static part. The scale matrix is expressed through a constant variance $\overset{i}{\sigma}_u^2$, that modulates the noise, and the correlation matrix $\overset{i}{\boldsymbol{\Gamma}}{}^{\mathrm{u}}$ defining the spatial structure of that noise. In the examples of

265   applications presented in Sec. **??**, both $\overset{i}{\boldsymbol{\Gamma}}$ and $\overset{i}{\boldsymbol{\Gamma}}{}^{\mathrm{u}}$ are obtained as analytical functions of the spatial coordinates. In Algorithm 4, $\overset{i}{\boldsymbol{\Gamma}}$ and $\overset{i}{\boldsymbol{\Gamma}}{}^{\mathrm{u}}$ have been specified through Gaussian functions, other possibilities for correlation functions have been described for instance by **?**. We have chosen not to inflate or deflate $\mathbf{P}^{\mathrm{f}}$ directly and to modulate the amplitude of background covariances only through the terms of Eq. (5), this way we reduce the number of parameters that need to be specified. As a matter of fact, for the combination of observations and background in the analysis procedure, the m by m covariance matrices are never

270   directly used. Instead, the matrices used are: the covariances between grid points and observation locations, $\overset{i}{\mathbf{G}}{}^{\mathrm{b}} = \overset{i}{\mathbf{P}}{}^{\mathrm{b}} \overset{i}{\mathbf{H}}{}^{\mathrm{T}}$, specifically only the ith row of this matrix is used; and the covariances between observation locations $\overset{i}{\mathbf{S}}{}^{\mathrm{b}} = \overset{i}{\mathbf{H}} \overset{i}{\mathbf{P}}{}^{\mathrm{b}} \overset{i}{\mathbf{H}}{}^{\mathrm{T}}$. $\overset{i}{\mathbf{H}}$ is the local observation operator, that is a linear function: $\mathbb{R}^m \to \mathbb{R}^{p_i}$.

The local observation error covariance matrix $\overset{i}{\mathbf{R}}$ is written as the constant observation error variance $\overset{i}{\sigma}_o^2$ multiplying the correlation matrix $\overset{i}{\boldsymbol{\Gamma}}{}^{\mathrm{o}}$:

275    $$\overset{i}{\mathbf{R}} = \overset{i}{\sigma}_o^2 \overset{i}{\boldsymbol{\Gamma}}{}^{\mathrm{o}} \tag{7}$$

$\overset{i}{\boldsymbol{\Gamma}}{}^{\mathrm{o}}$ often is the identity but other choices are possible. For instance, if some observations are know to be more accurate than the average of the others, then the corresponding diagonal elements of $\overset{i}{\boldsymbol{\Gamma}}{}^{\mathrm{o}}$ can be set to values smaller than 1. The observation uncertainty can vary in time and space, accordingly to ~~WA1~~P1, however its spatial structure is fixed and depends on the analytical function chosen for $\overset{i}{\boldsymbol{\Gamma}}{}^{\mathrm{o}}$. Note that the observation error is not determined by the instrumental error only but it

280   includes the representativeness error (**??**), which is often the largest component of the observation error. The representative error is a consequence of the mismatch between the spatial supports of the areal averages reconstructed by the background and the almost point-like observations.

The spatial structures of the error covariance matrices are determined through the matrices in Eqs. (5)- (6). At this point, we need to ~~scale the covariances to satisfy our WA2 and the first step is to define the background error variance in a way that is in~~

285   ~~line with WA3. We prefer to specify the ratio between variances instead of the variances themselves. Then, we introduce the~~ ~~global variable~~ set $\overset{i}{\sigma}_u^2$ and $\overset{i}{\sigma}_o^2$ to scale the magnitude of the covariances. In the process described below we will see that the

two variances are completely determined by two scalars ε^2 ~~as:~~

$$\varepsilon^2 = \overset{i}{\sigma}_o^2 / \overset{i}{\sigma}_b^2$$

~~where~~ and ν, also defined below, that we assume to be known before running the spatial analysis. This prior knowledge defines

290   the constraints that the solution has to satisfy and allows us to choose one particular solution among all the possibilities. $\overset{i}{\sigma}_u^2$ and $\overset{i}{\sigma}_o^2$ characterize the region around the ith grid point as a whole, without distinguishing between the individual observations. We introduce two relationships linking $\overset{i}{\sigma}_u^2$ and $\overset{i}{\sigma}_o^2$ through two additional variances, both expressing uncertainty of a quantity over the same region around the ith grid point: $\overset{i}{\sigma}_b^2$ is the average background error variance~~in the surroundings of the ith grid point.~~ ; $\overset{i}{\sigma}_f^2$ is the average forecast error variance. The two relationships are:

295    $$\varepsilon^2 \;\eqsim\; \overset{i}{\sigma}_o^2 / \overset{i}{\sigma}_b^2 \tag{8}$$

$$\overset{i}{\sigma}_b^2 \;\eqsim\; \overset{i}{\sigma}_f^2 + \overset{i}{\sigma}_u^2 \tag{9}$$

ε^2 is ~~used to express the level of confidence we have in~~ a global variable and it is the relative precision of the observations with respect to the background~~and it~~. Eq. (7) implements P3 and ε^2 should be set to a value smaller than ~~1 (WA3).~~ 1. For example, $\varepsilon^2 = 0.1$ means that we believe the observations to be ten times more precise an estimate of the true value than the background.

300   ~~The definition of $\overset{i}{\sigma}_b^2$~~ Eq. (8) is an adaptation from Eq. (5)~~:~~.

$$\overset{i}{\sigma}_b^2 = \overset{i}{\sigma}_f^2 + \overset{i}{\sigma}_u^2$$

~~where the average forecast error variance at the ith grid point $\overset{i}{\sigma}_f^2$ is defined as:~~

$$\overset{i}{\sigma}_f^2 = \alpha \; \langle \mathrm{diag}\left(\overset{i}{\mathbf{S}}^{\mathrm{f}} \right) \rangle = \alpha \; \frac{1}{p_i} \sum_{j=1}^{p_i} \overset{i}{\mathbf{S}}^{\mathrm{f}}{}_{jj}$$

~~The mean over an ensemble of similar realizations $\langle \ldots \rangle$ is interpreted as the mean over the diagonal elements of $\overset{i}{\mathbf{S}}^{\mathrm{f}}$. diag $(\ldots)$~~

305   ~~stands for the vector composed by the diagonal elements of the matrix in parentheses. α is a stabilization factor introduced to make the estimation of~~. The next two relationships we introduce have the objective to estimate $\overset{i}{\sigma}_f^2$ ~~more robust. A proper estimation~~ and the empirical (i.e. based on data, not on theories) estimate of $\overset{i}{\sigma}_{ob}^2$ which is the sum of $\overset{i}{\sigma}_o^2$ plus $\overset{i}{\sigma}_b^2$ directly from the forecasts and the observed values. $\overset{i}{\sigma}_{ob}^2$ is used to get a reference value to judge if the ensemble spread is adequate. The equations are (the averaging operator $\langle \ldots \rangle$ is defined as in Algorithm 4):

310    $$\overset{i}{\sigma}_f^2 \;\eqsim\; \nu \; \langle \mathrm{diag}\left(\overset{i}{\mathbf{S}}^{\mathrm{f}} \right) \rangle \tag{10}$$

$$\overset{i}{\sigma}_{ob}^2 \;\eqsim\; \nu \; \langle \left(\overset{i}{\mathbf{y}}^{\mathrm{o}} - \overset{i}{\mathbf{y}}^{\mathrm{b}} \right)^2 \rangle \tag{11}$$

ν is an inflation factor that can be used to get better results (e.g. via optimization of cross-validation scores or other verification metrics). In addition to that, ν is introduced because Eq. (10) is sensitive to misbehaviour in the data when applied using data

from one single timestep. Proper estimates of $\overset{i}{\sigma}_f^2$ and $\overset{i}{\sigma}_{ob}^2$ would require more than just one case, the ideal situation would be to ~~include in the average of Eq.~~ consider numerous situations characterized by similar weather conditions. ~~For the reasons discussed in WA5~~Instead, we prefer to ~~introduce α, which can be optimized as described in Sec. ??.~~

~~Considering the definition of $\overset{i}{\sigma}_b^2$ given by~~ stick to P5. The estimation of $\overset{i}{\sigma}_{ob}^2$ is not resistant, in the sense defined by **?**. A few outliers in ~~Eq.~~ ~~, we can proceed with the implementation of WA2. The background values at observation locations are $\overset{i}{\mathbf{y}}^{\mathrm{b}} = \overset{i}{\mathbf{H}\mathbf{x}}^{\mathrm{b}}$. WA2 is realized by imposing that the sum of observation and background error variances in the surroundings of a point is proportional to the local mean squared innovation (i. e.observations minus background), that is:~~

$$\overset{i}{\sigma}_{ob}^2 = \overset{i}{\sigma}_o^2 + \overset{i}{\sigma}_b^2 = \alpha \left\langle \left(\overset{i}{\mathbf{y}}^{\mathrm{o}} - \overset{i}{\mathbf{y}}^{\mathrm{b}} \right)^2 \right\rangle$$

~~a similar equation~~ (10) may have a significant impact on $\overset{i}{\sigma}_{ob}^2$. The introduction of ν makes the estimation procedure more resilient in the presence of outliers and other non-standard behaviour. Eq. (10) is used for diagnostics in ~~DA (**?**). In~~ data assimilation (**?**) and it is consistent with P2. The combination of Eq. ~~, the same stabilization factor α introduced for~~ (7) and Eq. ~~has been used, since the reasons that lead to the use of a stabilization factor are the same in both equations and we want to have as few parameters as possible to optimize. By substituting Eqs. ~~ (10) returns a rough empirical estimate of $\overset{i}{\sigma}_b^2$ that is:

$$\overset{i}{\sigma}_{b'}^2 = \nu \, \frac{\left\langle \left(\overset{i}{\mathbf{y}}^{\mathrm{o}} - \overset{i}{\mathbf{y}}^{\mathrm{b}} \right)^2 \right\rangle}{1+\varepsilon^2} \tag{12}$$

As a final step, to set $\overset{i}{\sigma}_u^2$ and $\overset{i}{\sigma}_a^2$ we distinguish between three situations. The first situation is when the ensemble spread is likely to underestimate the actual uncertainty because the background is missing an event or the spread is too narrow. The test condition is $\overset{i}{\sigma}_f^2 < \overset{i}{\sigma}_{b'}^2$. We will refer to this situation as the ensemble being overconfident or underdispersive. This is the case when a positive $\overset{i}{\sigma}_u^2$ is needed in Eq. (5) and we set its value such that $\overset{i}{\sigma}_b^2$ in Eq. (8) ~~into~~ is equal to $\overset{i}{\sigma}_{b'}^2$ in Eq. ~~, the value of $\overset{i}{\sigma}_u^2$ that satisfies Eq. is obtained as~~ (**??**):

$$\overset{i}{\sigma}_u^2 \;\equiv\; \overset{i}{\sigma}_{b'}^2 - \overset{i}{\sigma}_f^2 = \nu \left[\langle (\overset{i}{\mathbf{y}}^{\mathrm{o}} - \overset{i}{\mathbf{y}}^{\mathrm{b}})^2 \rangle / (1+\varepsilon^2) - \mathrm{diag}(\overset{i}{\mathbf{S}}^{\mathrm{f}}) \right] \tag{13}$$

$$\overset{i}{\sigma}_b^2 \;\equiv\; \nu \, \langle (\overset{i}{\mathbf{y}}^{\mathrm{o}} - \overset{i}{\mathbf{y}}^{\mathrm{b}})^2 \rangle / (1+\varepsilon^2) \tag{14}$$

$$\overset{i}{\sigma}_o^2 \;\equiv\; \varepsilon^2 \, \nu \, \langle (\overset{i}{\mathbf{y}}^{\mathrm{o}} - \overset{i}{\mathbf{y}}^{\mathrm{b}})^2 \rangle / (1+\varepsilon^2) \tag{15}$$

The second situation is when the ensemble spread is consistent with the empirical estimate of $\overset{i}{\sigma}_b^2$. The test condition is $\overset{i}{\sigma}_f^2 \geq \overset{i}{\sigma}_{b'}^2$ and $\overset{i}{\sigma}_f^2 > 0$. We will refer to this situation as the ensemble spread being adequate. In this case the background

475 "Felles aktiviteter NVE-MET 2019-2020 tilknyttet nasjonal flom- og skredvarslingstjeneste".
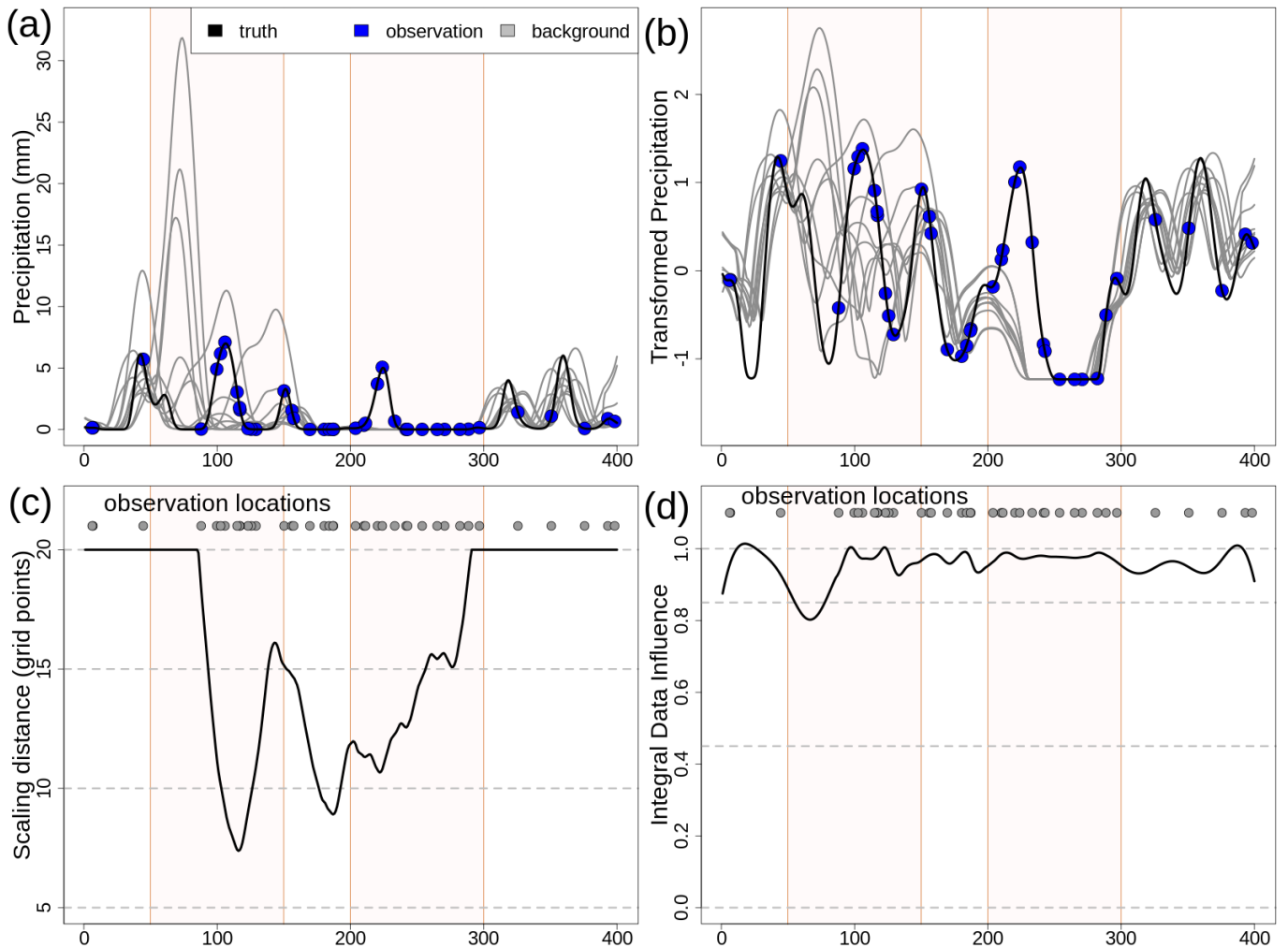
Figure 1. One-dimensional simulation. Panel *a*, precipitation (mm): truth (black line), observations (blue dots) and background (gray lines). Panel *b*, transformed values. Panel *c*, reference length scale for the scale matrix D_i (units u, as defined in Sec. **??**), D_i is bounded within 3 u and 20 u. Panel *d*, Integral Data Influence (IDI) based on D_i from panel *c*. The two regions R1 and R2 have been highlighted with a shaded color in the background of each panel.

Panel *a* shows the background. Panels *b-d* show the analysis with the different configurations.

Table 1. Overview of variables and notation for global variables. All the vectors are column vectors if not otherwise specified. If $\mathbf{X}$ is a matrix, $\mathbf{X}_i$ is its ith column (column vector) and $\mathbf{X}_{i,:}$ is its ith row (row vector).

symbol	description	space	dimension
m	number of grid points	-	~~-~~scalar
p	number of observations	-	~~-~~scalar
k	number of forecast ensemble members	-	~~-~~scalar
$\tilde{\mathbf{X}}^{\mathrm{f}}$	forecast ensemble	original	mxk matrix
$\mathbf{X}^{\mathrm{f}}$	forecast ensemble	transformed	mxk matrix
$\mathbf{x}^{\mathrm{f}}$	forecast ensemble mean	transformed	p vector
$\mathbf{A}^{\mathrm{f}}$	forecast perturbations	transformed	mxk matrix
$\mathbf{P}^{\mathrm{f}}$	forecast covariance matrix	transformed	mxm matrix
$\tilde{\mathbf{y}}^{\mathrm{o}}$	observations	original	p vector
$\mathbf{y}^{\mathrm{o}}$	observations	transformed	p vector
$\tilde{\mathbf{x}}^{\mathrm{t}}$	truth	original	m vector
$\mathbf{x}^{\mathrm{t}}$	truth	transformed	m vector
$\tilde{\mathbf{x}}^{\mathrm{a}}$	analysis	original	m vector
$\mathbf{x}^{\mathrm{a}}$	analysis	transformed	m vector
$\boldsymbol{\eta}^{\mathrm{a}}$	analysis error	transformed	m vector
$\mathbf{P}^{\mathrm{a}}$	analysis error covariance matrix	transformed	mxm matrix
$\boldsymbol{\sigma}^{\mathrm{a}}$	analysis error standard deviation, $\sqrt{\mathrm{diag}\left(\mathbf{P}^{\mathrm{a}}\right)}$	transformed	m vector
$\mathbf{x}^{\mathrm{b}}$	background	transformed	m vector
$\boldsymbol{\eta}^{\mathrm{b}}$	background error	transformed	m vector
$\mathbf{P}^{\mathrm{b}}$	background error covariance matrix	transformed	mxm matrix
$\boldsymbol{\varepsilon}^{\mathrm{o}}$	observation error	transformed	p vector
$\mathbf{H}$	observation operator	transformed	pxm matrix
$\mathbf{L}$	reference length scales for localization	transformed	m vector
$\mathbf{D}$	reference length scales of the scale matrix	transformed	m vector
ε^2	relative quality of the background wrt observations	transformed	~~-~~scalar
~~α~~ ν	~~stabilization coefficient~~ inflation factor	transformed	~~-~~scalar
ξ	small constant	original	scalar
α_D	shape of the gamma PDF used in the data transformation	original	scalar
β_D	rate of the gamma PDF used in the data transformation	original	scalar
$\boldsymbol{\alpha}^{\mathrm{a}}$	shape of the analysis gamma PDF	original	m vector
$\boldsymbol{\beta}^{\mathrm{a}}$	rate of the analysis gamma PDF	original	m vector

Table 2. Overview of variables and notation for local variables. All variables are specified in the transformed space. All the vectors are column vectors if not otherwise specified. If $\mathbf{X}$ is a matrix, $\mathbf{X}_i$ is its ith column (column vector) and $\mathbf{X}_{i,:}$ is its ith row (row vector).

| symbol	description	dimension
p_i	number of observations in the surroundings of the ith grid point	scalar
$\overset{i}{\mathbf{H}}$	observation operator	p_ixm matrix
$\overset{i}{\mathbf{R}}$	observation error covariance matrix	p_ixp_i matrix
$\overset{i}{\mathbf{\Gamma}}^{\mathrm{o}}$	observation error correlation matrix	p_ixp_i matrix
$\overset{i}{\mathbf{y}}^{\mathrm{b}}$	background at observation locations	p_i vector
$\overset{i}{\mathbf{P}}^{\mathrm{b}}$	background error covariance matrix	mxm matrix
$\overset{i}{\mathbf{\Gamma}}$	localization matrix	mxm matrix
$\overset{i}{\mathbf{V}}$	localization between grid points and observation locations	mxp_i matrix
$\overset{i}{\mathbf{Z}}$	localization between observation locations	p_ixp_i matrix
$\overset{i}{\mathbf{\Gamma}}^{\mathrm{u}}$	scale correlation matrix	mxm matrix
$\overset{i}{\mathbf{G}}^{\mathrm{b}}$	background error covariances between grid points and observation locations	mxp_i matrix
$\overset{i}{\mathbf{S}}^{\mathrm{b}}$	background error covariances between observation locations	p_ixp_i matrix
$\overset{i}{\mathbf{G}}^{\mathrm{f}}$	forecast error covariances between grid points and observation locations	mxp_i matrix
$\overset{i}{\mathbf{S}}^{\mathrm{f}}$	forecast error covariances between observation locations	p_ixp_i matrix
$\overset{i}{\sigma}_o^2$	observation error variance	scalar
$\overset{i}{\sigma}_b^2$	average background error variance	scalar
$\overset{i}{\sigma}_{b\prime}^2$	empirical estimate of $\overset{i}{\sigma}_b^2$	scalar
$\overset{i}{\sigma}_f^2$	average forecast error variance	scalar
$\overset{i}{\sigma}_u^2$	error variance for the scale matrix	scalar
$\overset{i}{\sigma}_{ob}^2$	sum of error variances (Eq. (10))	scalar
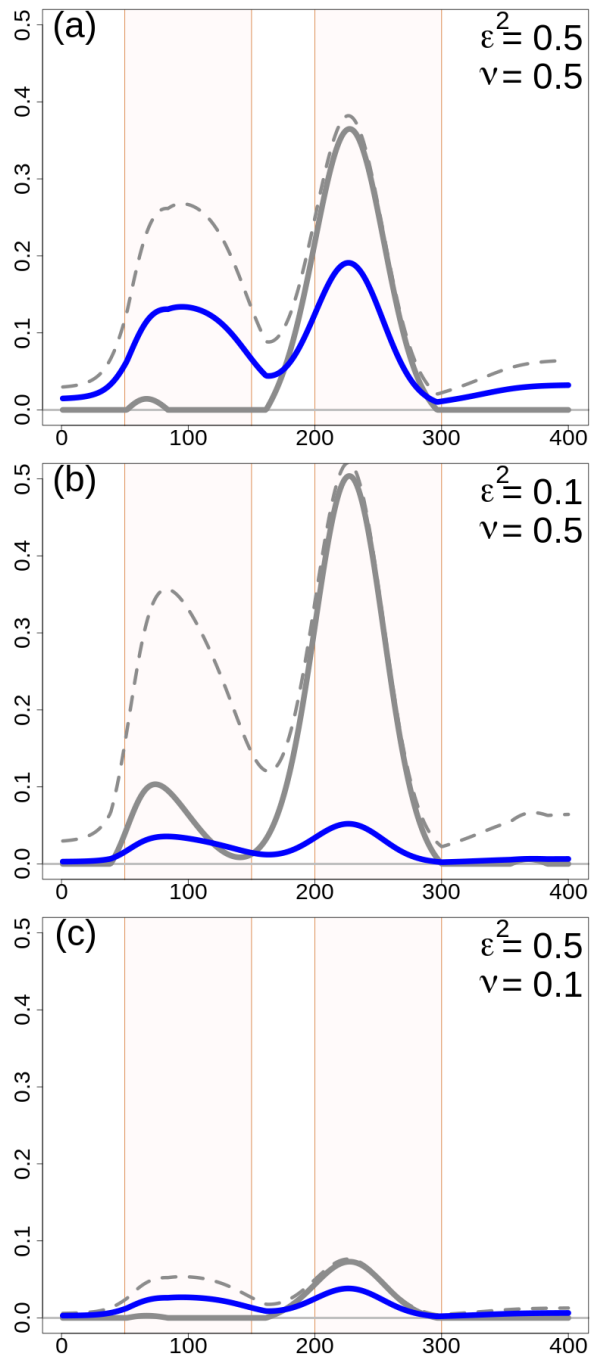
Figure 2. One-dimensional simulation~~in the transformed precipitation space. Analyses at grid points with~~ Error variances (dimensionless quantities) for different configurations of the scaling parameters. The variances shown are: $\overset{i}{\sigma}{}^{2}_{u}$ thick gray line; $\overset{i}{\sigma}{}^{2}_{b}$ dashed gray line; $\overset{i}{\sigma}{}^{2}_{o}(=\varepsilon^{2}\overset{i}{\sigma}{}^{2}_{b})$ blue line. $\overset{i}{\sigma}{}^{2}_{t}$ is the difference between $\overset{i}{\sigma}{}^{2}_{b}$ and $\overset{i}{\sigma}{}^{2}_{u}$. For all panels ~~: $\varepsilon^{2}=0.1$, $L=25$~~ u in $\overset{i}{\Gamma}$ and the error variances do not depend on choices on $\overset{i}{\Gamma}$ or $\overset{i}{\Gamma^{u}}$. Panel a ~~: $\overset{i}{\Gamma^{u}}$ with Gaussian function, $\alpha=0.1$~~ $\varepsilon^{2}=0.5$ and $\nu=0.5$. Panel b ~~: $\overset{i}{\Gamma^{u}}$ with Gaussian function, $\alpha=1.0$~~ $\varepsilon^{2}=0.1$ and $\nu=0.5$. Panel c ~~: $\overset{i}{\Gamma^{u}}$ with exponential function, $\alpha=0.1$. Panel d: $\overset{i}{\Gamma^{u}}$ with exponential function, $\alpha=1.0$. For each panel, the red line is the analysis (expected value), the pink area shows the interval between the 90th~~ $\varepsilon^{2}=0.5$ and ~~the 10th percentiles, the gray dots~~ $\nu=0.1$. The two regions R1 and ~~lines are~~ R2 have been highlighted with a shaded color in the ~~observations and backgrounds, respectively (see~~ background of each panel~~b in Fig. 1)~~.
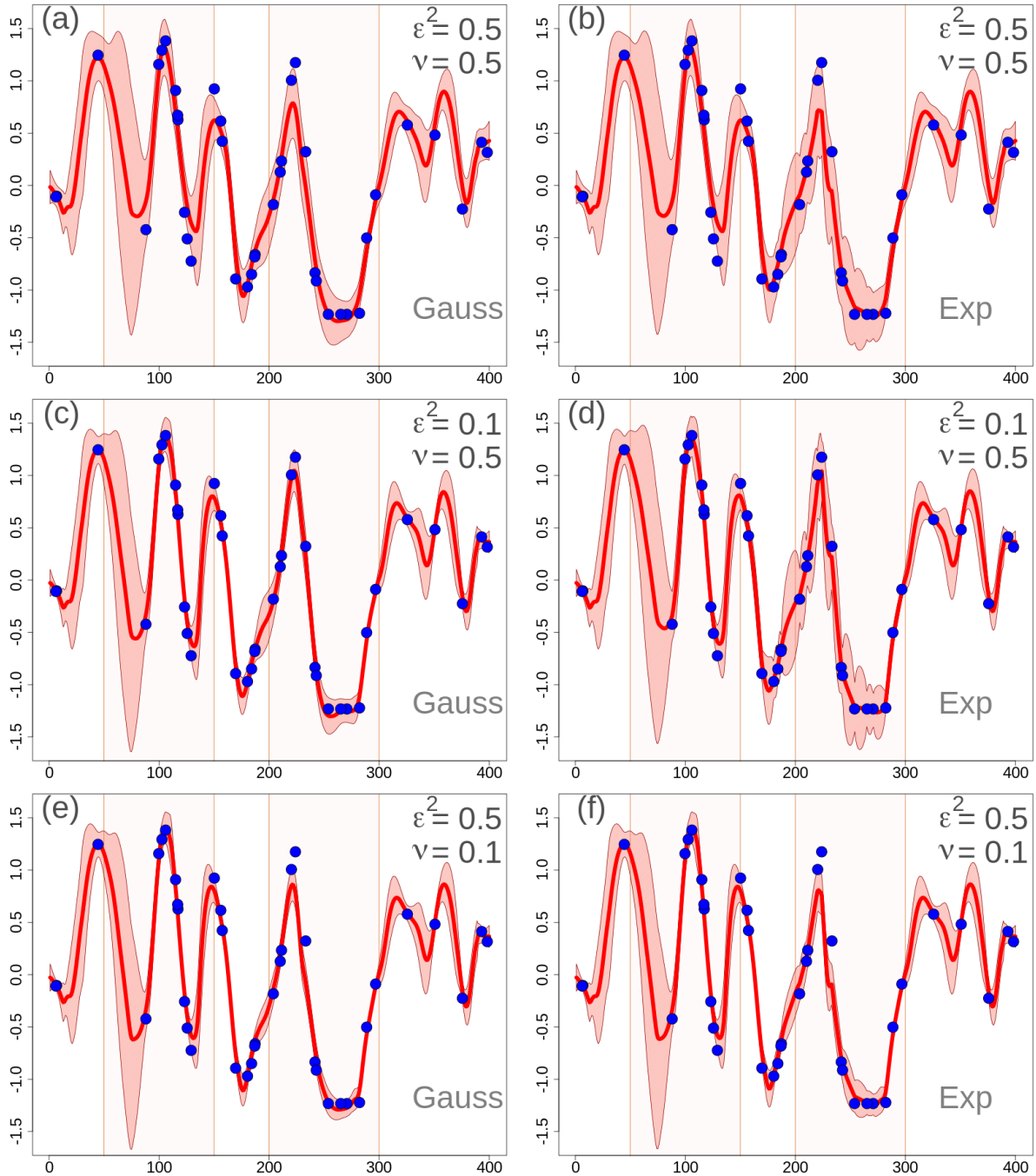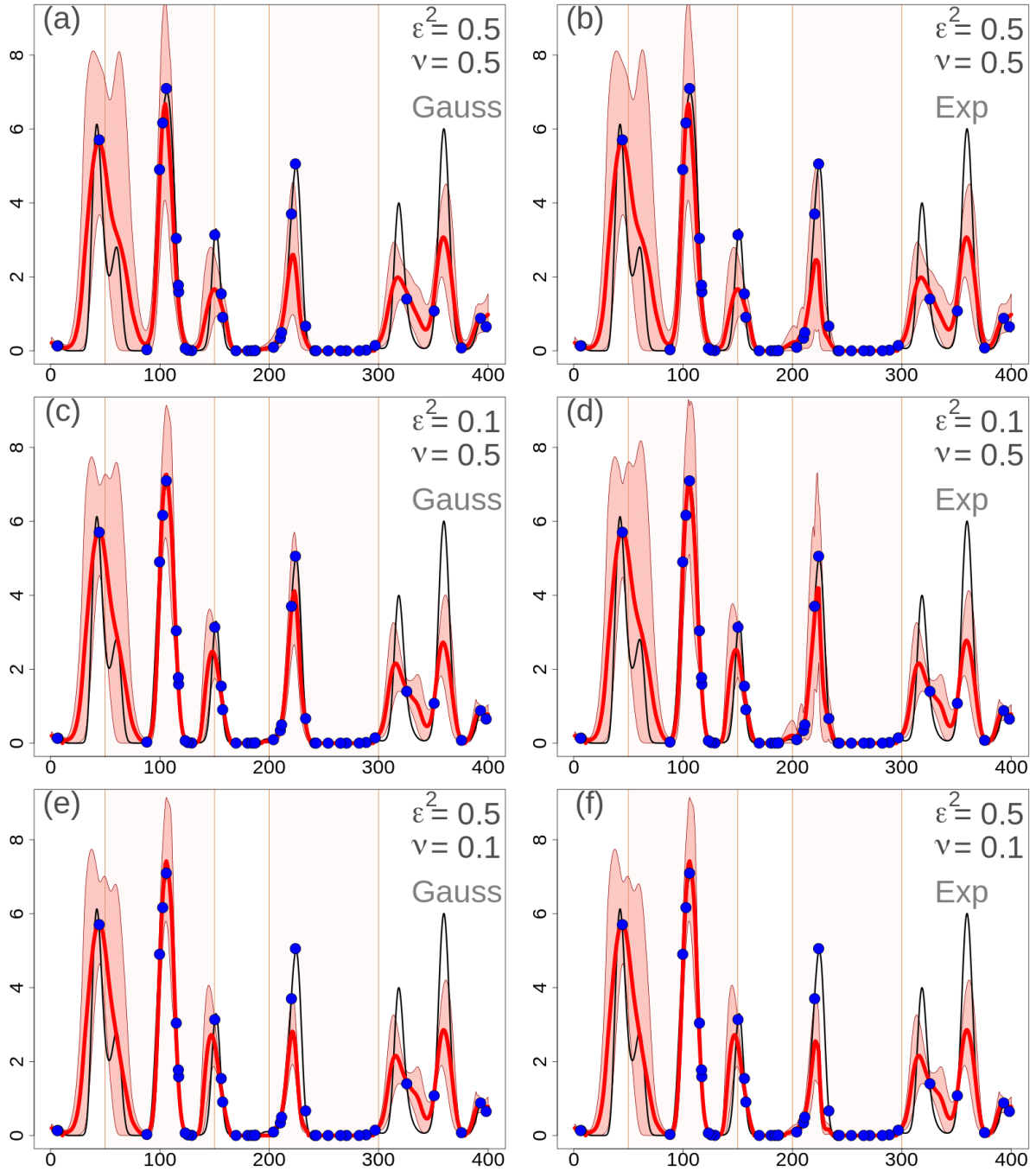
16

Figure 3. One-dimensional simulation in the transformed precipitation space. Analyses at grid points with different EnSI-GAP configurations. For all panels $L = 25\,u$. The values of ν and ε^2 are reported in the panels. Specification of the scale matrix $\overset{i}{\mathbf{\Gamma}^{\mathrm{u}}}$: the panels on the left column have been obtained with a Gaussian function, while the panels on the right column with an exponential function. For each panel, the red line is the analysis (expected value), the pink area shows the interval between the 90th and the 10th percentiles, the blue dots are the observations as in Fig. 1*b*. The two regions R1 and R2 have been highlighted with a shaded color in the background of each panel.
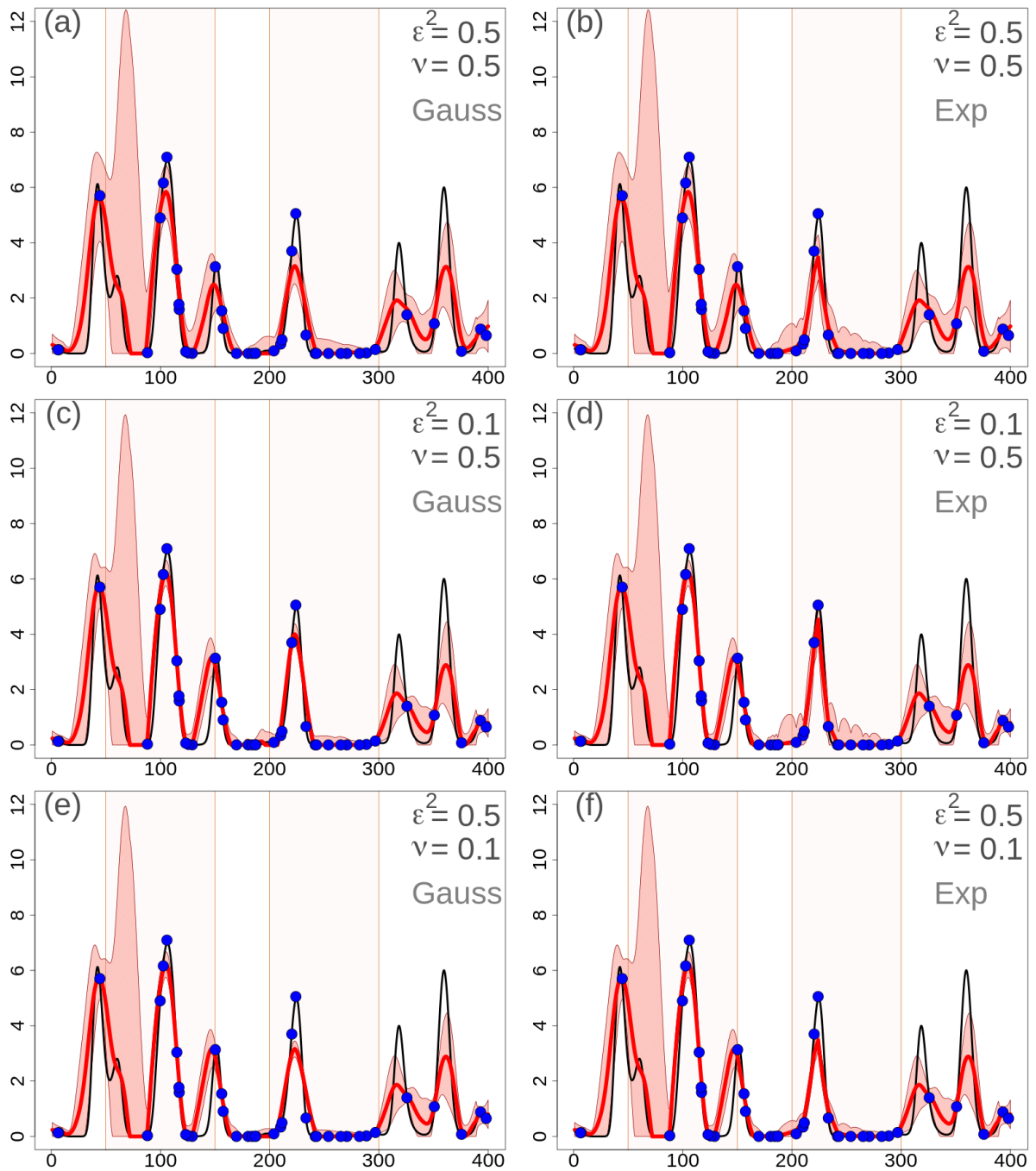
Figure 4. One-dimensional simulation in the original precipitation space (mm). Analyses at grid points with different EnSI-GAP configurations. For all panels: $\varepsilon^2 = 0.1$, $L = 25\,u$. The red line is the analysis (expected value), the pink area shows the 90th-10th percentile, the black line layout is the truth. Panels *a-d* same as in Fig. 2. Panel *e*: no data transformation, Γ^u_i with Gaussian function, $\alpha = 0.1$. Panel *f*: no data transformation, Γ^u_i with Gaussian function, $\alpha = 1.0$. Note the different scale for precipitation between panels *e-f* and the others**??**.

18

Figure 5. One-dimensional simulation in the original precipitation space (mm). Analyses at grid points with different EnSI-GAP configurations without applying the data transformation.. The layout is the same as in Fig. **??**.
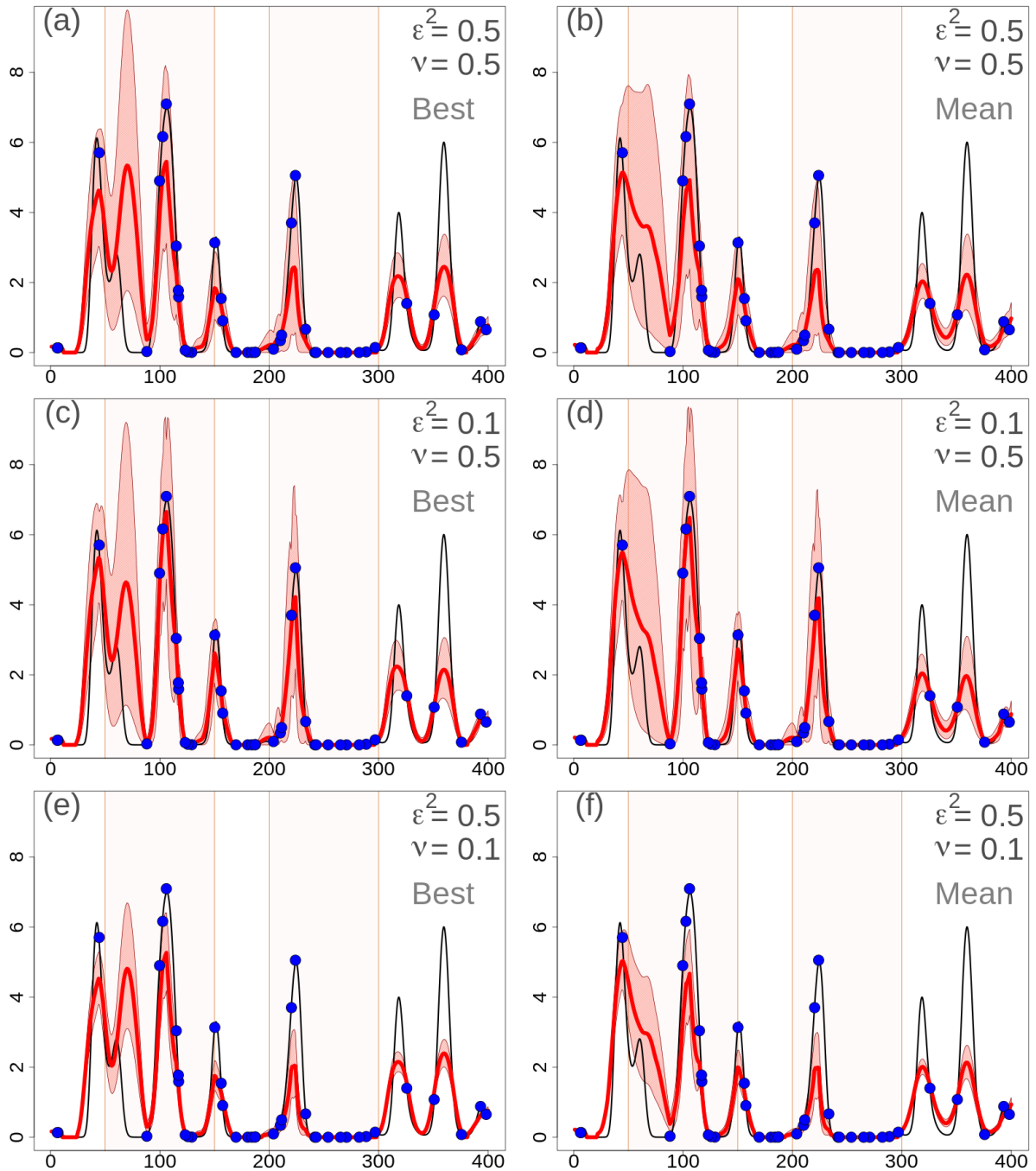
Figure 6. One-dimensional simulation ~~in the original precipitation space (mm)~~. ~~Error variances obtained~~ Analyses at grid points with different EnSI-GAP configurations ~~. The variances shown are: $\overset{i}{\sigma}{}^2_o(=\varepsilon^2\overset{i}{\sigma}{}^2_b)$, blue line; $\overset{i}{\sigma}{}^2_b$, black thick line; $\overset{i}{\sigma}{}^2_u$, black dashed line; $\overset{i}{\sigma}{}^2_f$ as~~ without considering the ~~difference between $\overset{i}{\sigma}{}^2_b$ and $\overset{i}{\sigma}{}^2_u$~~ whole ensemble. ~~For all panels: $\alpha=1$, $L=25u$ and~~ Specification of the scale matrix $\overset{i}{\mathbf{\Gamma}}{}^{\mathrm{u}}$ ~~with Gaussian~~ through an exponential function. ~~Panel a (dimensionless quantities): Gaussian anamorphosis, $\varepsilon^2=0.1$. Panel b (dimensionless quantities): Gaussian anamorphosis, $\varepsilon^2=1.0$ $\overset{i}{\mathbf{\Gamma}}{}^{\mathrm{f}}$ is not used. Panel c (mm^2): no data transformation, $\varepsilon^2=0.1$~~ The layout is similar to Fig. ~~Panel d (mm^2): no data transformation~~ **??** except that here the panels in the left column show the results obtained considering as the background the best member of the ensemble, ~~$\varepsilon^2=1.0$~~ while in the right column the background is the ensemble mean.
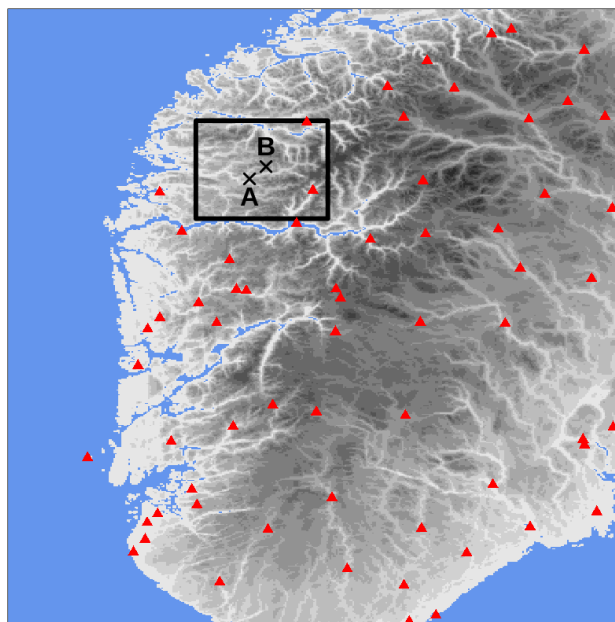
Figure 7. "South Norway" domain used in the simulations of Secs. **??**- **??**. The red triangles mark station locations used for cross-validation in Sec. **??**. The gray shades indicate the altitude (from the lighter gray at 0 m to the darker gray at approximately 2400 m a.m.s.l.). The blue shade indicates the sea. The black box delimits the "Sogn og Fjordane" domain shown in ~~Fig~~Figs. 10- 8, the crosses mark the two points A and B used in the following.
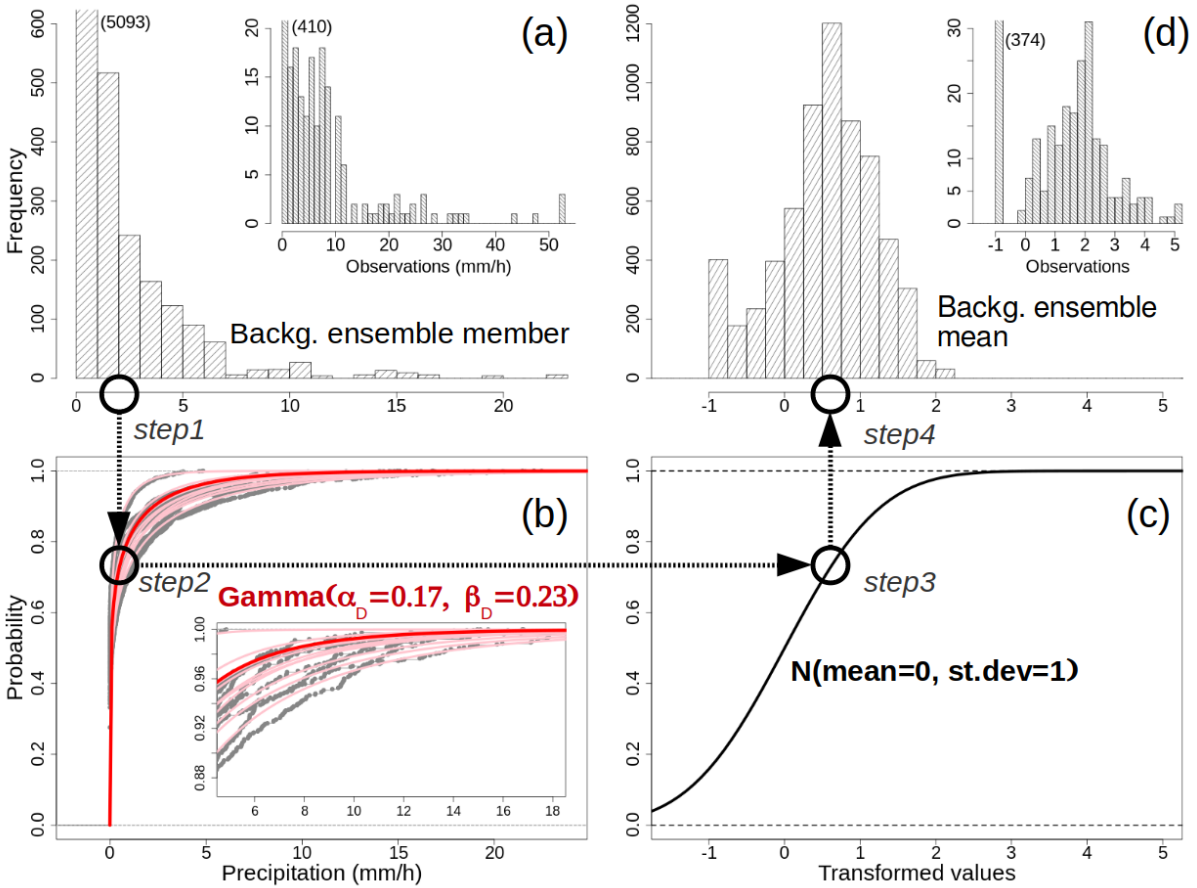
Figure 8. Data transformation procedure, example for 2019-07-30 15:00 UTC hourly precipitation totals over Sogn og Fjordane (see Fig. 5). Panel *a* shows the histograms with the frequencies of occurrence for: one member of the ensemble forecast and the observed values. The numbers in round brackets indicate the values of the truncated bins. Panel *b* shows the cumulative distribution functions (CDFs) for the 10 forecast ensemble members: the empirical CDFs are shown with gray dots, the best-fitting Gamma CDFs are shown as pink lines. The final Gamma CDF used in the Gaussian anamorphosis is shown with the red line and the parameters are reported. The inset on the bottom right shows an enlargement of a section of the main graph. Panel *c* shows the standard Gaussian CDF. Panel *d* shows the distributions of transformed values for the background ensemble mean and the observations. The 4 different steps of the data transformation for an arbitrary value of precipitation (approximately 2 mm/h) are indicated by circles and arrows.
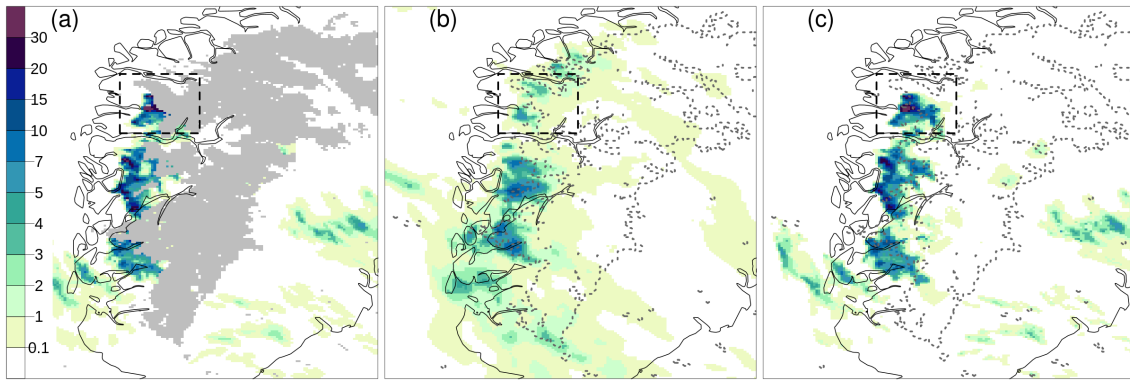
Figure 9. 2019-07-30 15:00 UTC, hourly precipitation totals (mm/h) over South Norway (see Fig. 5). Observations are shown in panel *a* over the same grid as the analysis. For each grid cell, the average of the observed values within the cell is shown. Grid points that are not covered by observations are marked in gray in panel *a* and the dashed gray lines in panels *b* and *c* delineate the boundary of the gray area shown in panel *a*. The background ensemble mean is shown in panel *b*. The analysis expected value is shown in panel *c*. The color scale is the same for all panels. The "Sogn og Fjordane" domain of Fig. 5 is shown as the dashed box.
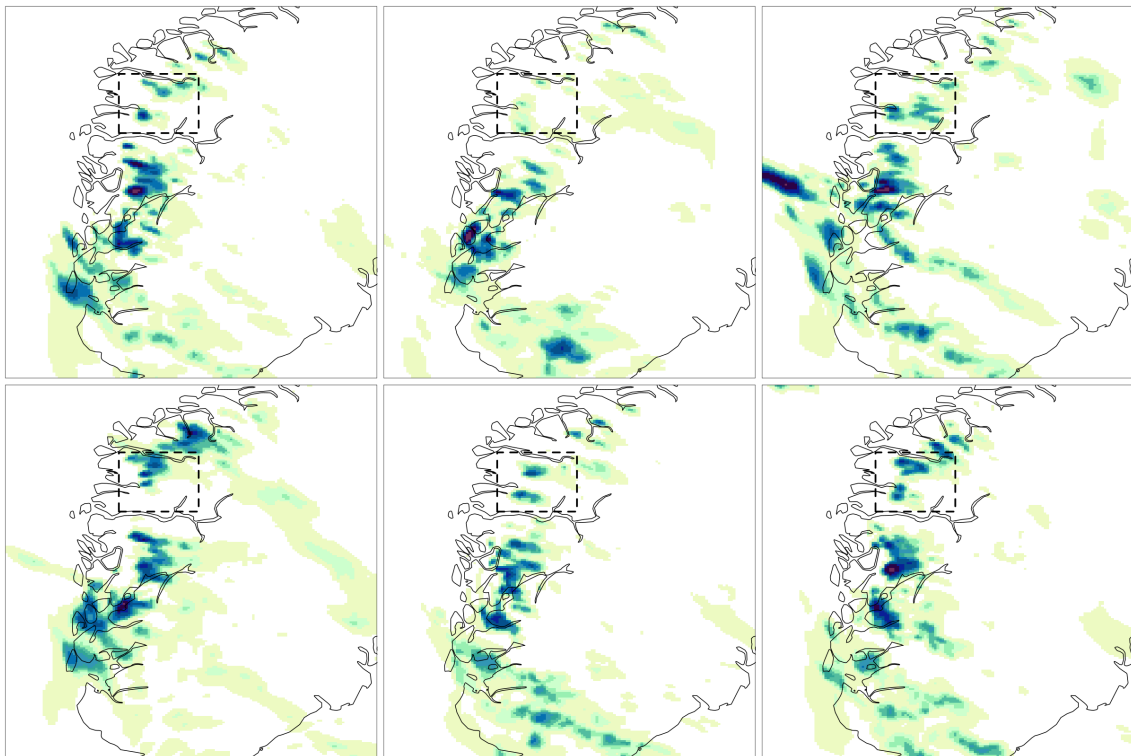

Figure 10. 2019-07-30 15:00 UTC, hourly precipitation totals (mm/h) over South Norway (see Fig. 5) for six of the ten background ensemble members. The color scale is the same as in Fig. 6. The "Sogn og Fjordane" domain of Fig. 5 is shown as the dashed box.
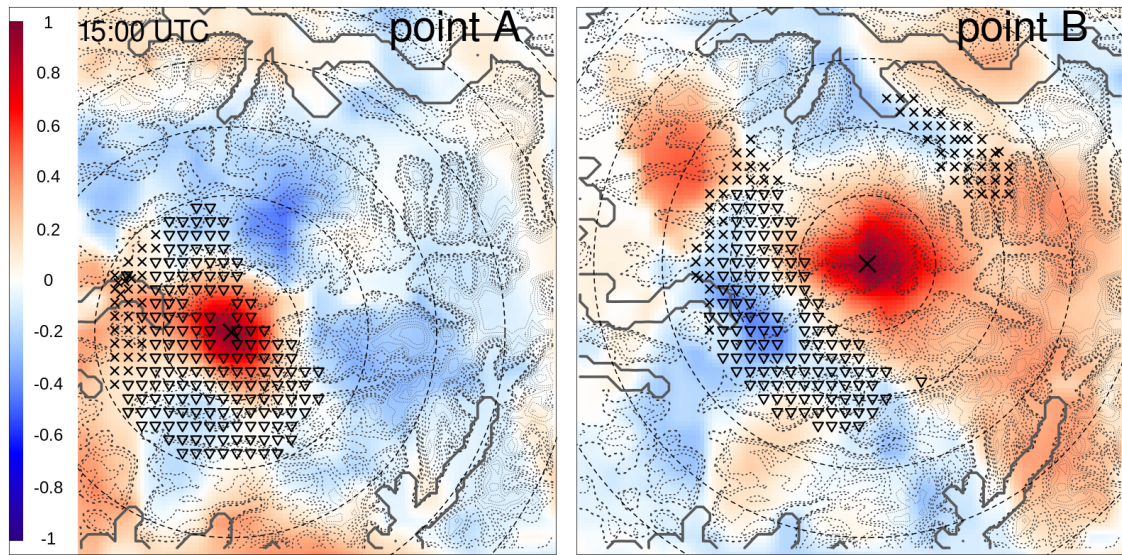
Figure 11. 2019-07-30 15:00 UTC, background error correlations $\mathbf{\Gamma}^{\mathrm{b}}{}_{i,i}^{i}$ of Eq. **(??)** used for spatial analysis of hourly precipitation totals over Sogn og Fjordane (see Fig. 5). The blue-red color shades show the background error correlations. With reference to Fig. 5, the left panel shows the background error correlations between point A and the grid points. For point B, the correlations are shown in the right panel. The symbols show the closest 200 observations, the triangles are observations of precipitation, while the crosses are observations of no-precipitation. The concentric circles have their common center at either point A or B and they are distance isolines at: 10 km, 20 km, 30 km, 40 km and 50 km. The thick dark gray lines delimit the fjords. The dashed lines are the contour lines for elevation: the thickest mark the 500 m isoline, the others have a gradually smaller thickness for 600 m, 700 m, 900 m, 1000 m, 1100 m, 1200 m, 1300 m, 1400 m, 1500 m.
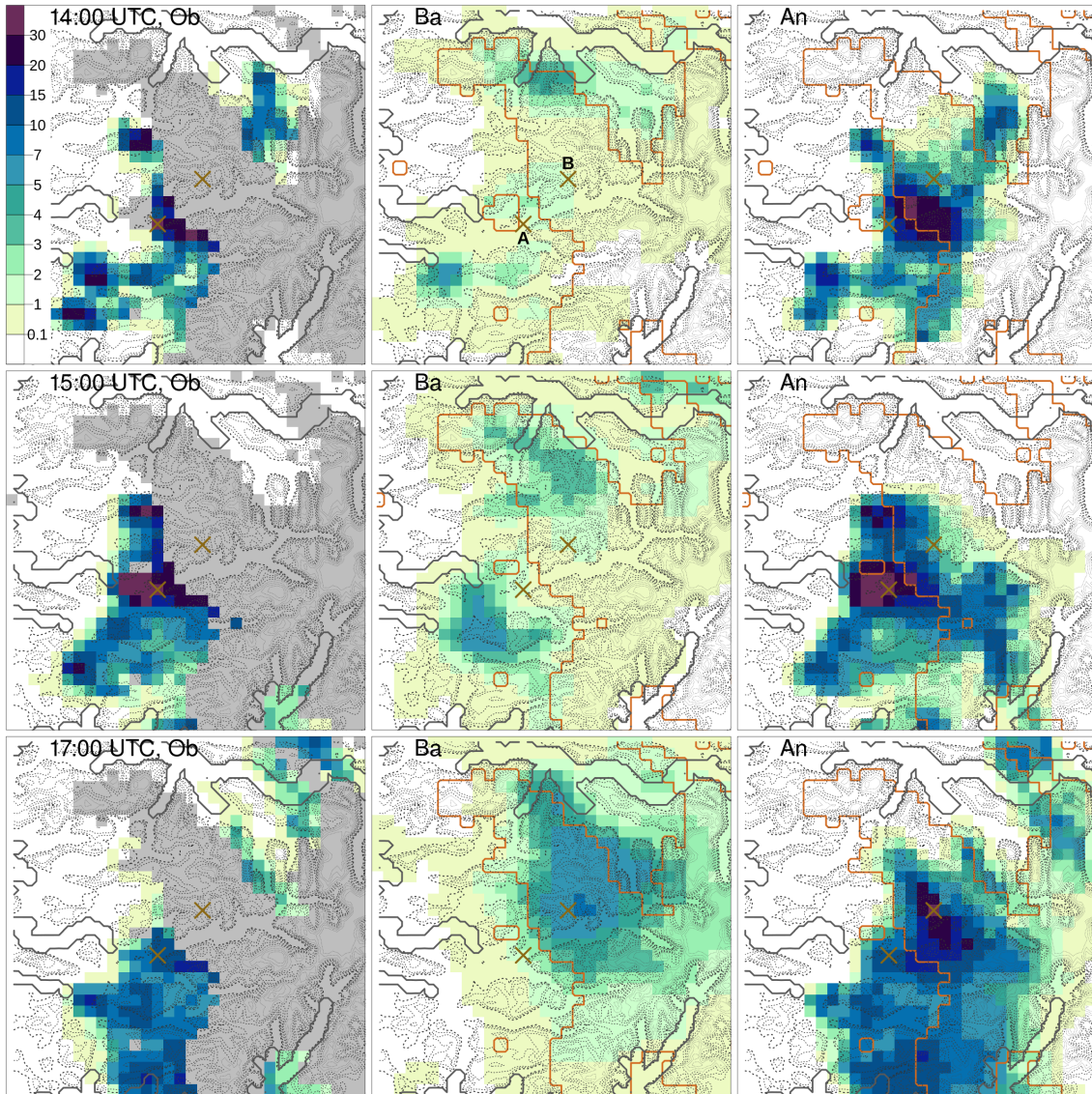
Figure 12. 2019-07-30 14:00 UTC (top row), 15:00 UTC (middle row), 17:00 UTC (bottom row) hourly precipitation totals (mm/h) over Sogn og Fjordane (see Fig. 5). The panels labeled with *Ob* (left column) show the aggregated observed values, as in Fig. 6. The panels with *Ba* (middle column) show the background ensemble mean. The panels with *An* (right column) show the analysis expected value. The crosses mark the A and B points of Fig. 5, which are also shown in the middle panel of the top row. The dark orange lines in panels *Ba* and *An* delineate the boundary of the gray area shown in panel *Ob*. The color scale is the same for all panels. The thick lines and the dashed lines have the same meaning as in Fig. 10.
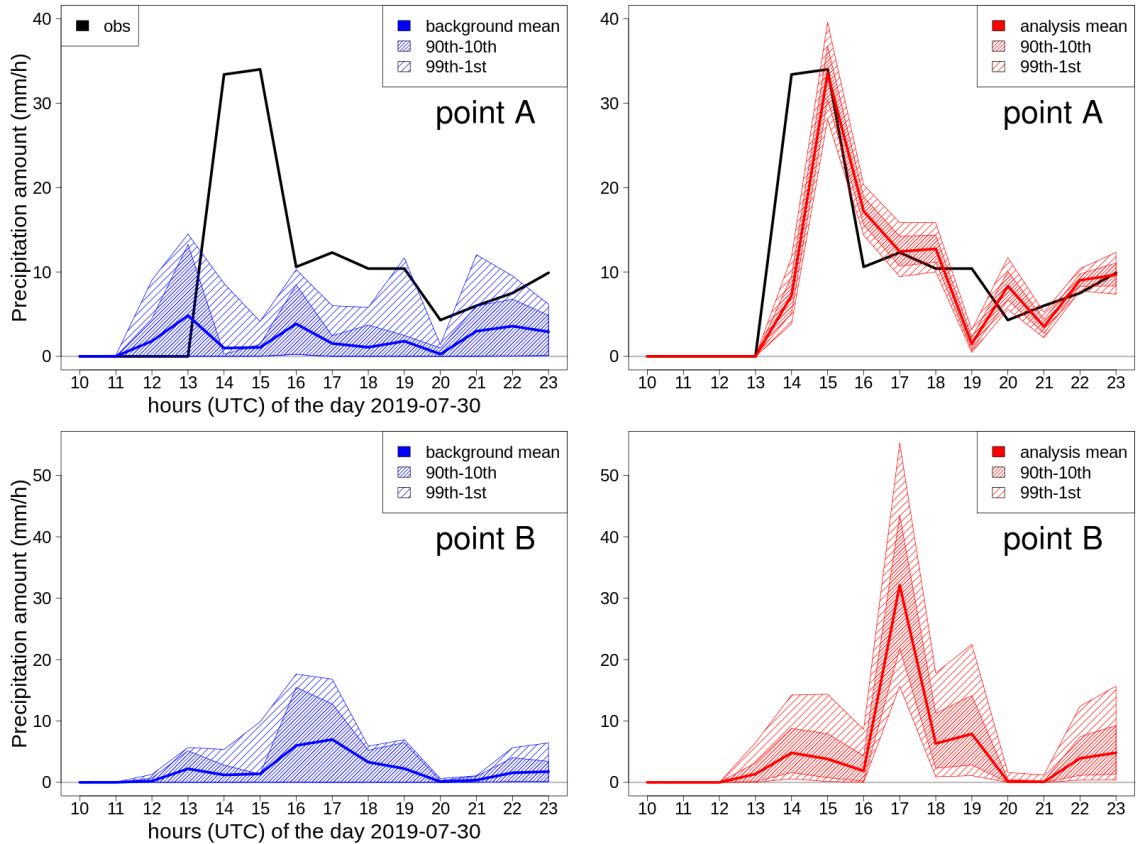
Figure 13. Time series of hourly precipitation totals for the period 2019-07-30 10:00 UTC to 23:00 UTC at points A (top row) and B (bottom row) of Fig. 5. The left panels show the background (blue). The right panels show the analysis (red). The blue (red) line shows the background (analysis) mean, the region with denser shading lines is the difference between the 90th and the 10th percentiles, the region with sparser shading lines is the difference between the 99th and the 1st percentiles. For point A, the closest observation, which is a radar-derived estimate, is shown (black line). Point B is in a region where observations are not available.

Figure 14. Summer 2019 hourly precipitation statistics for the cross-validation experiments. Panels: *a* background versus observations; *b* analysis $\varepsilon^2 = 1$ ~~$\alpha = 1$~~ $\nu = 1$ versus observations; *c* analysis $\varepsilon^2 = 0.1$ ~~$\alpha = 0.1$~~ $\nu = 0.1$ versus observations; *d* analysis $\varepsilon^2 = 1.0$ ~~$\alpha = 0.1$~~ $\nu = 0.1$ versus observations. The independent observations have been divided into classes, the number of samples within each class is shown in the inset of panel *a*. Within each class and for each probabilistic prediction, several percentiles have been computed. The regions between the average of the 90th and the 10th percentiles are shown by light gray shades. The regions between the average of the 75th and the 25th percentiles are shown by dark gray shades. The thick black line indicates the average of the medians. The dashed black line is the diagonal (1:1) line. The angular coefficients of the best-fitting lines passing through the origins and better approximating the averages of the medians are shown, for the background in panel *a* it is 0.26 (not shown in the panel).

27

Figure 15. Equitable Threat Score (ETS) for summer 2019 hourly precipitation, as obtained through the cross-validation experiments. The black lines are the ETS curves for the analysis mean values, as indicated in the legend. The ETS curve for the background is the gray line. The precipitation thresholds defining the "yes" events are reported on the x-axis.
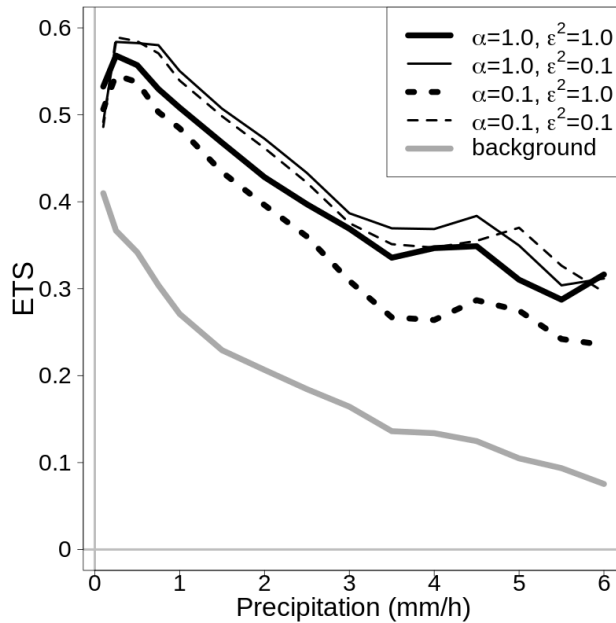
Table 3. Summary statistics on the evaluation of the 100 one-dimensional simulations. Results are presented for three modes: EnSI-GAP; "no transformation", which is EnSI-GAP without applying the Gaussian anamorphosis; "no ensemble", which is EnSI-GAP where the background is the ensemble mean and the background error covariance matrix is determined solely by the scale matrix. The configurations listed are the same that have been used in Figs. **??**- 4 and the abbreviations have the same meanings (e.g., with reference to Fig. **??**, the first row corresponds to panel a, the second to panel b and so on). The mean-squared error skill score (MSESS, Eq. (**??**)) is positively oriented with a perfect score being 1. The continuous ranked probability score ($\overline{\text{CRPS}}$, Eq. (**??**)) is negatively oriented with a perfect score being 0. For each configuration and score, the best values are marked with bold fonts.

Mode	EnSI-GAP		no transformation		no ensemble	
Configuration	MSESS	$\overline{\text{CRPS}}$	MSESS	$\overline{\text{CRPS}}$	MSESS	$\overline{\text{CRPS}}$
$\varepsilon^2 = 0.5, \nu = 0.5$, Gauss	**0.66**	**0.80**	**0.66**	0.91	0.63	0.95
$\varepsilon^2 = 0.5, \nu = 0.5$, Exp	0.65	**0.78**	**0.68**	0.85	0.65	0.81
$\varepsilon^2 = 0.1, \nu = 0.5$, Gauss	**0.70**	**0.79**	0.68	0.95	0.65	1.01
$\varepsilon^2 = 0.1, \nu = 0.5$, Exp	0.71	0.72	0.71	0.80	**0.73**	**0.71**
$\varepsilon^2 = 0.5, \nu = 0.1$, Gauss	0.66	**0.92**	**0.67**	1.04	0.61	1.33
$\varepsilon^2 = 0.5, \nu = 0.1$, Exp	0.63	**0.92**	**0.68**	0.98	0.61	1.14

forecast ensemble $\tilde{\mathbf{X}}^{\mathrm{f}}$ and ensemble mean $\mathbf{x}^{\mathrm{f}}$; observations $\tilde{\mathbf{y}}^{\mathrm{o}}$; parameters ε^2, $\alpha\nu$, $\mathbf{L}$, $\mathbf{D}$

Gaussian anamorphosis: estimation of α_D and β_D, then $\mathbf{X}^{\mathrm{f}} = g(\tilde{\mathbf{X}}^{\mathrm{f}})$; $\mathbf{y}^{\mathrm{o}} = g(\tilde{\mathbf{y}}^{\mathrm{o}})$

480   Define additional global variables: $\mathbf{x}^{\mathrm{b}} = \mathbf{x}^{\mathrm{f}}$; $\mathbf{A}^{\mathrm{f}}$: $\mathbf{A}_i^{\mathrm{f}} = \mathbf{X}_i^{\mathrm{f}} - \mathbf{x}^{\mathrm{f}}$

grid points $i = 1, \ldots, m$

select the closest p_i observations $\overset{i}{\mathbf{y}}{}^{\mathrm{o}}$ and obtain $\overset{i}{\mathbf{y}}{}^{\mathrm{b}} = \overset{i}{\mathbf{H}}\mathbf{x}^{\mathrm{b}}$

Dynamical background error covariance matrices, $\overset{i}{\mathbf{S}}{}^{\mathrm{f}} \approx (k-1)^{-1}(\overset{i}{\mathbf{H}}\overset{i}{\mathbf{\Gamma}}\overset{i}{\mathbf{H}}{}^{\mathrm{T}}) \circ [(\overset{i}{\mathbf{H}}\mathbf{A}^{\mathrm{f}})(\overset{i}{\mathbf{H}}\mathbf{A}^{\mathrm{f}})^{\mathrm{T}}]$

$\overset{i}{\mathbf{Z}}$: $\overset{i}{\mathbf{Z}}_{jl} = \exp\left\{-0.5\left[d\left(\mathbf{r}_j, \mathbf{r}_l\right)/L_i\right]^2\right\}, j = 1, \ldots, p_i$ and $l = 1, \ldots, p_i$; $d()$ horizontal distance

485   $\overset{i}{\mathbf{S}}_{jl}^{\mathrm{f}} \approx (k-1)^{-1}\overset{i}{\mathbf{Z}}_{jl}[(\overset{i}{\mathbf{H}}\mathbf{A}^{\mathrm{f}})_{j,:}(\overset{i}{\mathbf{H}}\mathbf{A}^{\mathrm{f}})_{l,:}], j = 1, \ldots, p_i$ and $l = 1, \ldots, p_i$

$\overset{i}{\mathbf{G}}_{i,:}^{\mathrm{f}} \approx (k-1)^{-1}(\overset{i}{\mathbf{\Gamma}}\overset{i}{\mathbf{H}}{}^{\mathrm{T}})_{i,:} \circ [\mathbf{A}_{i,:}^{\mathrm{f}}(\overset{i}{\mathbf{H}}\mathbf{A}^{\mathrm{f}})^{\mathrm{T}}]$

$\overset{i}{\mathbf{V}}_{i,:}$: $\overset{i}{\mathbf{V}}_{il} = \exp\left\{-0.5\left[d\left(\mathbf{r}_i, \mathbf{r}_l\right)/L_i\right]^2\right\}, l = 1, \ldots, p_i$

$\overset{i}{\mathbf{G}}_{i,l}^{\mathrm{f}} \approx (k-1)^{-1}\overset{i}{\mathbf{V}}_{il}[\mathbf{A}_{i,:}^{\mathrm{f}}(\overset{i}{\mathbf{H}}\mathbf{A}^{\mathrm{f}})_{l,:}], l = 1, \ldots, p_i$

Background error covariance matrices

490   definition of $\langle \ldots \rangle$: $\langle \mathbf{c} \rangle = \sum_{l=1}^{p_i}(\overset{i}{\mathbf{V}}_{il}\mathbf{c}_l)/\sum_{l=1}^{p_i}(\overset{i}{\mathbf{V}}_{il})$, where $\mathbf{c}$ is a generic p_i vector

$\overset{i}{\sigma}_f^2 = \nu\langle\mathrm{diag}(\overset{i}{\mathbf{S}}{}^{\mathrm{f}})\rangle$; $\overset{i}{\sigma}_{ob}^2 = \nu\left\langle(\overset{i}{\mathbf{y}}{}^{\mathrm{o}} - \overset{i}{\mathbf{y}}{}^{\mathrm{b}})^2\right\rangle$

$(\overset{i}{\sigma}_{ob}^2 = 0)$ and $(\overset{i}{\sigma}_f^2 = 0)$

$\mathbf{x}_i^{\mathrm{a}} = \mathbf{x}_i^{\mathrm{b}}$, then apply the inverse data transformation $\tilde{\mathbf{x}}_i^{\mathrm{a}} = g^{-1}(\mathbf{x}_i^{\mathrm{a}})$ and STOP

$[\overset{i}{\sigma}_{ob}^2/(1+\varepsilon^2)] \leq \overset{i}{\sigma}_f^2$

495   $\overset{i}{\sigma}_u^2 = 0$; $\overset{i}{\mathbf{S}}{}^{\mathrm{b}} = \overset{i}{\mathbf{S}}{}^{\mathrm{f}}$; $\overset{i}{\mathbf{G}}_{i,:}^{\mathrm{b}} = \overset{i}{\mathbf{G}}_{i,:}^{\mathrm{f}}$

$\overset{i}{\sigma}_u^2 = \overset{i}{\sigma}_{ob}^2/(1+\varepsilon^2) - \overset{i}{\sigma}_f^2$

add the scale matrix $\overset{i}{\sigma}_u^2\overset{i}{\mathbf{\Gamma}}{}^{\mathrm{u}}$ to the background error covariance matrices

$\overset{i}{\mathbf{S}}{}^{\mathrm{b}}$: $\overset{i}{\mathbf{S}}_{jl}^{\mathrm{b}} = \overset{i}{\mathbf{S}}_{jl}^{\mathrm{f}} + \overset{i}{\sigma}_u^2\exp\left\{-0.5\left[d\left(\mathbf{r}_j, \mathbf{r}_l\right)/D_i\right]^2\right\}, j = 1, \ldots, p_i$ and $l = 1, \ldots, p_i$

$\overset{i}{\mathbf{G}}_{i,:}^{\mathrm{b}}$: $\overset{i}{\mathbf{G}}_{il}^{\mathrm{b}} = \overset{i}{\mathbf{G}}_{il}^{\mathrm{f}} + \overset{i}{\sigma}_u^2\exp\left\{-0.5\left[d\left(\mathbf{r}_i, \mathbf{r}_l\right)/D_i\right]^2\right\}, l = 1, \ldots, p_i$

500   Observation error covariance matrix: first $\overset{i}{\sigma}_b^2 = \overset{i}{\sigma}_f^2 + \overset{i}{\sigma}_u^2$, then $\mathrm{diag}(\overset{i}{\mathbf{R}}) = \varepsilon^2 \overset{i}{\sigma}_b^2$

Analysis

$\mathbf{x}_i^{\mathrm{a}} = \mathbf{x}_i^{\mathrm{b}} + \overset{i}{\mathbf{G}}_{i,:}^{\mathrm{b}}(\overset{i}{\mathbf{S}}{}^{\mathrm{b}} + \overset{i}{\mathbf{R}})^{-1}\left(\overset{i}{\mathbf{y}}{}^{\mathrm{o}} - \overset{i}{\mathbf{y}}{}^{\mathrm{b}}\right)$

$(\boldsymbol{\sigma}^2)_i^{\mathrm{a}} = \mathbf{P}_{ii}^{\mathrm{f}} + \overset{i}{\sigma}_u^2 - \overset{i}{\mathbf{G}}_{i,:}^{\mathrm{b}}(\overset{i}{\mathbf{S}}{}^{\mathrm{b}} + \overset{i}{\mathbf{R}})^{-1}(\overset{i}{\mathbf{G}}_{i,:}^{\mathrm{b}})^{\mathrm{T}}$

Data back transformation

505   inverse transformation g^{-1} of 400 quantiles of the distribution $N\left(\mathbf{x}_i^{\mathrm{a}}, (\boldsymbol{\sigma}^2)_i^{\mathrm{a}}\right)$ $\boldsymbol{\alpha}_i^{\mathrm{a}}$ and $\boldsymbol{\beta}_i^{\mathrm{a}}$ are obtained by optimizing the

fitting of a gamma distribution to the 400 quantiles through a least squares fitting method